Daksh Jangra

INTERACTION ANALYSIS AND CONTROLLER DESIGN FOR SINGLE- INDUCTOR DOUBLE-OUTPUT DC-DC BOOSTCONVER...

major project 2

Document Details

Submission ID

trn:oid:::27535:142403833

Submission Date

Jun 10, 2026, 11:25 AM GMT+5:30

Download Date

Jun 10, 2026, 11:28 AM GMT+5:30

File Name

Daksh Thesis Main Final (1).pdf

File Size

2.0 MB

65 Pages

12,575 Words

75,367 Characters

1% Overall Similarity

The combined total of all matches, including overlapping sources, for each database.

Filtered from the Report

- Bibliography
- Quoted Text
- Cited Text
- Small Matches (less than 12 words)

Match Groups

10 Not Cited or Quoted 1%
Matches with neither in-text citation nor quotation marks

0 Missing Quotations 0%
Matches that are still very similar to source material

0 Missing Citation 0%
Matches that have quotation marks, but no in-text citation

0 Cited and Quoted 0%
Matches with in-text citation present, but no quotation marks

Top Sources

1% Internet sources
1% Publications
1% Submitted works (Student Papers)

Match Groups

- **10** Not Cited or Quoted 1%
  Matches with neither in-text citation nor quotation marks
- **0** Missing Quotations 0%
  Matches that are still very similar to source material
- **0** Missing Citation 0%
  Matches that have quotation marks, but no in-text citation
- **0** Cited and Quoted 0%
  Matches with in-text citation present, but no quotation marks

Top Sources

1% Internet sources
1% Publications
1% Submitted works (Student Papers)

Top Sources

The sources with the highest number of matches within the submission. Overlapping sources will not be displayed.

1	Student papers	University of Bristol on 2025-04-30	<1%
2	Internet	joscex.shmpublisher.com	<1%
3	Internet	theses.lib.polyu.edu.hk	<1%
4	Publication	Manohar, Sujan Kundapur. "Techniques for efficient power management.", Proqu...	<1%
5	Student papers	Middle East Technical University on 2012-09-17	<1%
6	Student papers	University of Hong Kong on 2019-07-22	<1%
7	Publication	Yao Wang, Jianping Xu, Duo Xu. "Effect of Circuit Parameters on the Stability and ...	<1%
8	Internet	ir.nctu.edu.tw	<1%
9	Internet	researchrepository.murdoch.edu.au	<1%
10	Internet	www.mdpi.com	<1%

CHAPTER 1

INTRODUCTION

The constant development of power electronics has created an ever-increasing need for efficient power conversion technology that is also space-saving and economical. The increasing complexity of electronic equipment has made it essential that there be multiple regulated voltage supplies from one energy source. This has spurred research into novel converter structures that would be efficient yet simple and economical. Multi-output dc-dc converters represent an interesting option for this type of structure.

1.1 Motivation

The faster-growing adoption of renewable energy systems, electric vehicles, DC microgrids, telecommunication infrastructures, aerospace electronics, and portable devices has led to the increased demand for small-size and high-efficiency power conversion circuits. Electronic systems nowadays need different regulated voltage levels for operation. Traditional approaches include implementing multiple single-input single-output (SISO) converters separately generating independent output voltages. While such schemes are proven and reliable, they entail using a large number of magnetic components, switches, gate drivers, and controllers, which results in the increased converter size, power loss, cost, and implementation difficulty [20], [31], [49]. Multi-output DC–DC converters are promising solutions that allow increasing the power density in power supplies by merging multiple outputs into a single topology with multiple controlled outputs [20], [31]. Single-Inductor Double-Output (SIDO) converters are among the most effective multi-output DC–DC converters owing to the ability of generating two regulated outputs with a single shared inductor [9], [23], [39].

Having only one inductor minimizes the need for components and allows creating a more compact, cost-efficient, and effective converter. The SIDO converter is extensively employed in battery-based power sources, renewable energy sources, distributed power supplies, and embedded electronics [21], [41], [49]. Unfortunately, SIDO converters show strong couplings because two output channels work based on the same inductor.

Any change of one of the control inputs affects both output voltages causing mutual influences and couplings of channels [9], [10], [13]. Then, the SIDO DC–DC converter works as a MIMO system, and its channels interact strongly with each other. Such interactions increase the difficulty of designing controllers and adversely affect performance in the form of worse transient response, oscillations, instability, and disturbances rejection [1], [17].

Decentralized controllers design requires careful investigation of couplings to define proper input/output channels combinations. Bristol developed a method for calculating steady-state interaction in MIMO systems, namely, Relative Gain Array (RGA) method [1]. However, as power converters exhibit highly frequency dependent behavior, the information on steady-state couplings is not enough for designing a good controller. To compensate for this shortcoming, there are multiple methods of performing dynamic interaction analysis of power converters based on the Hankel Interaction Index Array (HIIA), approaches, Singular Value Decomposition (SVD), and H_2 norm interaction [3]–[6].

Several approaches to minimizing interaction of MIMO systems were introduced recently. They involve decentralized PID controllers, feedforward decoupling, sliding mode control, observer-based methods, robust control, and optimal multivariable control [11], [15], [28], [29], [35], [46]. Despite the numerous possible options of controlling SIDO converters, decentralized control based on PID algorithms remains popular due to simplicity, easy tuning and small number of calculations required [16], [19].

The present work focuses on interaction analysis and controller designed for a Single Inductor Double-Output boost converter system. The converter is made using small-signal state-space techniques and represented as a MIMO system. Various frequency-domain interaction analysis tools including Relative Gain Array (RGA), HIIA, singular value analysis, Nyquist analysis, and Bode analysis are employed for evaluating dynamic interaction characteristics. Based on the obtained interaction information, decentralized controller structures are designed and analyzed under different operating conditions. Comparative performance analysis of reference-tracking, disturbance-rejection, and balanced controller tuning approaches is also presented.

The primary purpose of the dissertation is to check the effect of interaction on the dynamics of the converter and to prove that an interaction-based control approach would lead to improved closed-loop characteristics of the SIDO system.

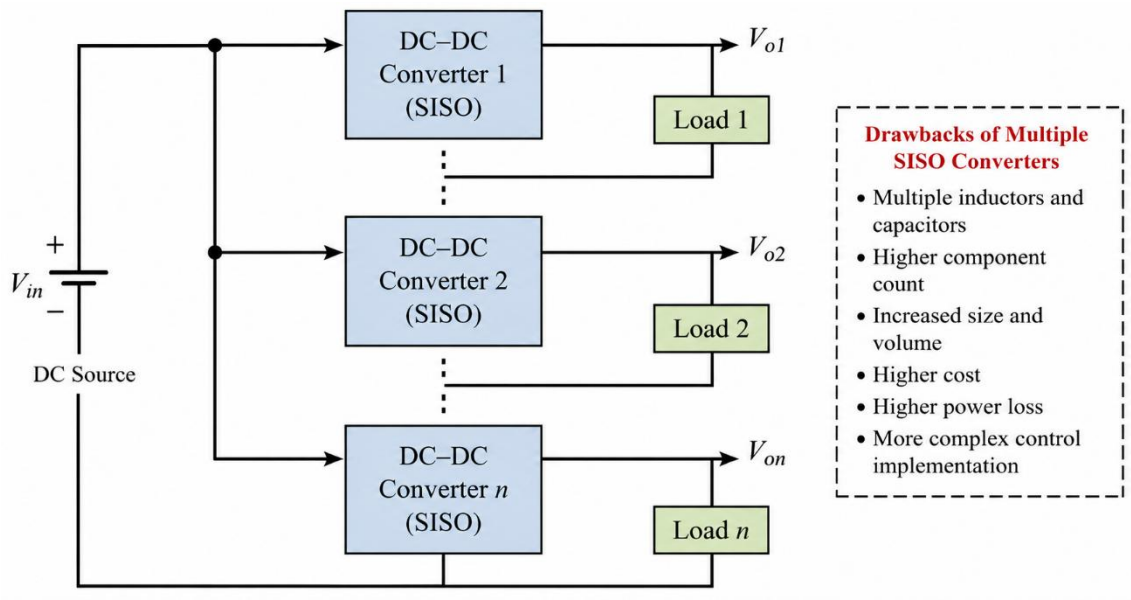

Figure 1.1 Conventional Multiple SISO Converter Structure

As shown in Figure 1.1, a traditional power conversion scheme employs SISO converters for producing various output voltages. Though independent control is possible, the use of multiple converter units adds complexity, converter volume, switching losses, and cost.

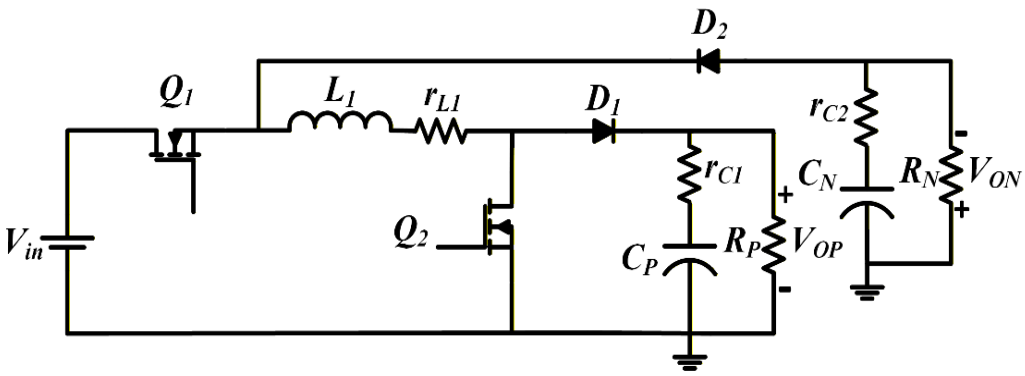

Figure 1.2 Single-Inductor Double-Output DC–DC Boost Converter

Figure 1.2 showing the configuration of a SIDO converter being analyzed in the dissertation. This particular converter makes use of a single inductor that transfers energy to both output ports. Because of the shared dynamics of the inductor, coupling occurs in the output channels.

This topology is distinguished by the utilization of a single common inductor as an energy storage device feeding two output channels. At the converter operation mode, energy is supplied to the inductor through respective switch turn-on. The energy is then delivered to respective output channel through a diode and corresponding switching pattern. Therefore, both output channels utilize a single inductor for energy storage and, therefore, require much fewer passive components than in conventional multi-converter structure.

Several benefits are provided by the utilization of the single common inductor. They include, but not limited to, reduction in converter size, component count, improvement in power density, decreased cost, and increased efficiency. These advantages make the SIDO converters promising for renewable energy system, battery supply, electric vehicle, telecommunication and distributed DC power system with multiple regulated voltages.

On the other hand, a single inductor results in certain problems. Namely, the two output channels are dependent on a common inductor current, thus, variations in duty ratio, load and reference voltage of one output channel affect the energy supply to another output channel, resulting in cross regulation and dynamic coupling between output channels. As such, the SIDO converter control is becoming quite complex because of these interactions.

Thus, it becomes important to provide proper mathematical modeling and analysis of the interaction in order to understand behavior of the SIDO converter and develop a suitable controller design approach. The modeling procedure, interaction analysis and control design algorithm will be described in the upcoming sections of this thesis.

1.2 Literature Review

This Multi-output DC–DC converter have received substantial attention owing to the capability of producing multiple regulated voltage levels through utilizing less physical hardware elements. The main features of single-inductor multiple-output converter topologies include smaller size of the converters, higher power density, reduced switching losses, and minimized passive element usage, as opposed to traditional multiple-converter configurations [20], [39], [49]. Various SIDO converter topologies have been reported for low-power electronics, distributed power, photovoltaics, and mobile devices [21]–[24]. The major drawback of SIDO converters includes interaction

between the different outputs due to the common inductor dynamics. Specifically, Dasika et al. [9] have studied the multivariable control problem in SIDO boost converters and have shown the presence of significant interaction between the control loops. Bahrani et al. [10] have considered the multivariable aspects of SIDO converters and illustrated that independent single-input single-output control approaches might result in unsatisfactory performances at dynamic operations. Other relevant references related to the issues of interaction and cross-regulation of multi-output converters have been introduced in [11]–[15].

The interaction analysis is crucial in multivariable controller design problems. In [1], Bristol has developed the Relative Gain Array (RGA) technique allowing to analyze this steady-state interaction and determine accurate input–output pairings for a multivariable system. However, static interaction analysis proves ineffective for power electronic converters owing to the very nature of such systems. Therefore, several interaction analysis techniques taking into account frequency-dependent behavior of power converters have been suggested in [3]–[6].

Specifically, these include various Hankel norms, Gramian matrices, and H_2 interaction measures. Several control techniques have been proposed for eliminating or reducing interaction effects and enhancing the voltage control performance of SIDO converters. Traditional PID controllers used in a decentralized fashion have proven to be widely applicable [16], [19]. Feedforward decoupling techniques have been proposed in [29] for reducing the influence of cross-coupling between output channels. Robust controller designs aimed at reducing interaction and providing enhanced disturbance suppression have been discussed in [15] and [46]. Also, observer-based control and sliding-mode control strategies have been proposed in [30], [35].

Although extensive literature can be found related to control of SIDO converters, few reports cover the interaction analysis and controller design combined. Specifically, the reported works are mostly dedicated either to SIDO converters' modelling or to designing the respective controllers without paying enough attention to the interaction aspects. Thus, performing comprehensive frequency-domain interaction analysis together with decentralized controller design for SIDO boost converters is still an important research direction.

1.3 Research Objectives

Following is the summary of the main purposes of this dissertation:

1. Design of the small-signal dynamic model of the Single-Inductor Double-Output (SIDO) Boost DC-DC converter.
2. Analysis of the interaction effects in the two channels of the converter through RGA, HIIA, and Singular Value methods.
3. Evaluation of different controller design methods to achieve stability and robustness in the converters.

1.4 Organization of Dissertation

This thesis is structured into 6 chapters. The first chapter contains the introduction, motivation, literature survey, and objectives of this thesis. Chapter second above discusses the topology and the working principle of Single Inductor Double Output of this Boost Converter system. Also presented are state-space modelling and small signal linearization of the converter system. Chapter 3 deals with the interaction analysis of the SIDO converter using Relative Gain Array (RGA), Higher Interaction Index Approach (HIIA), Singular Value Analysis, Bode Analysis, and Nyquist Analysis.

Chapter 4 explains decentralized control design methods for SIDO converter system. Methods such as reference tracking, disturbance rejection, and optimal controller tuning are explained. In Chapter 5, simulations are performed along with comparative analysis of the suggested controllers under various operating conditions such as variations in load and reference. Finally, the conclusion of the current research and future research directions for SIDO converters are discussed in Chapter 6. The sources referred to in the entire dissertation are listed in the last part of the thesis.

CHAPTER 2

SINGLE-INDUCTOR TWO-OUTPUT BOOST CONVERTER TOPOLOGY, OPERATION AND SMALL-SIGNAL MODELLING

2.1 Introduction

Single-Inductor Dual-Output (SIDO) DC–DC converters have gained a significant attention in recent years because of this compact structure, reducing component count, improved power density, and lower implementation cost. Unlike conventional multi-converter systems that require separate inductors and switching stages for generating multiple regulated outputs, SIDO converters utilize a single magnetic element for supplying power to multiple output channels simultaneously [7]-[10]. Consequently, the widespread usage of SIDO converters can be seen in portable electronic devices, telecommunication apparatuses, automotive electronics, renewable energy systems, and distributed DC power systems. Though, the employment of a single inductor increases the efficiency of the circuit, as well as reduces its physical dimensions, it causes the presence of interaction between the two output circuits. Since these both output channels share the same inductor current, any change in one channel affects the second output channel. This phenomenon is known as cross-regulation or interaction effect [11]-[14]. The presence of interaction significantly complicates controller design and stability analysis.

Therefore, the SIDO boost converter behaves as a Multi-Input Multi-Output (MIMO) system rather than an alone Single-Input Single-Output (SISO) system. Conventional independent controller design approaches are generally inadequate for such converters because they fail to account for dynamic coupling between output channels. Consequently, proper mathematical modelling and interaction analysis become essential for achieving satisfactory closed-loop performance.

This chapter represents the topology, operating principle, steady-state analysis, state-space modelling, small-signal transfer function derivation of the proposed SIDO boost converter. This derived mathematical model forms the basis for analysis and controller design presented in subsequent chapters.

2.2 Circuit Topology of the Proposed SIDO Boost Converter

The proposed Single-Inductor Dual-Output boost converter considered in this dissertation is shown in Fig. 2.1.

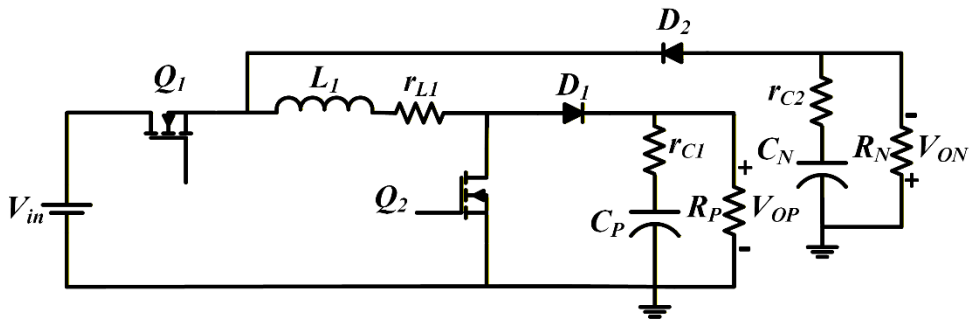

Fig. 2.1 Circuit Diagram of SIDO Boost Converter

The converter consists of:

- 1 DC input source V_{in},
- 2 shared inductor L,
- 2 controlled switches,
- 2 diodes,
- 2 output capacitors $C_1$and C_2,
- load resistors here are $R_1$and R_2.

Two output voltages, $V_a$and V_b, are generated by the SIDO DC-DC boost converter using two separate duty cycles, $d_1$and d_2, respectively. Using a single common inductor makes this design highly compact and efficient, as there are fewer parts needed and lower switching losses in comparison with the traditional converters. On the other hand, since both the outputs depend on the same inductor, any change in the energy provided by one output will automatically affect the other one as well. Hence, there is high coupling between the two output voltages in terms of their stability.

5 The converter parameters used in this simulation and modelling are in Table 2.1.

TABLE 2.1 CONVERTER PARAMETERS

Components	Symbols	Parameters
Inductor	L	470 µH
Capacitors	C_1, C_2	220 µF, 220 µF
Resistors	R_1, R_2	48 Ω, 36 Ω
Input Voltage	V_{in}	12 V
Output Voltages	V_a, V_b	24 V, 18 V
Load Currents	I_a, I_b	0.5 A, 0.5 A
Switching Frequency	f_s	50 kHz

2 The converter operates in Continuous Conduction Mode (CCM), where the inductor current remains continuous throughout the switching cycle.

2.3 Principle of Operation

The operation of the proposed SIDO boost converter is based on controlled charging and discharging of the common inductor. Depending upon the switching states of the power switches, energy stored in the inductor is distributed between the two output channels.

Since both outputs share the same inductor current, the energy transfer process inherently produces interaction between output channels. Therefore, any change in duty cycle associated with one output also affects the second output channel.

The converter operation during one switching cycle can be explained using four operating modes.

2.3.1 Mode I Operation

At this time, Q1 gets turned ON whereas Q2 remains OFF. The energy is provided to the inductor from the input source and hence gets stored within the magnetic field of the inductor. With rising current in the inductor, both diodes are reverse-biased and thus the output energy is zero. Thus at this instant, energy is fed to the output by the output capacitor only.

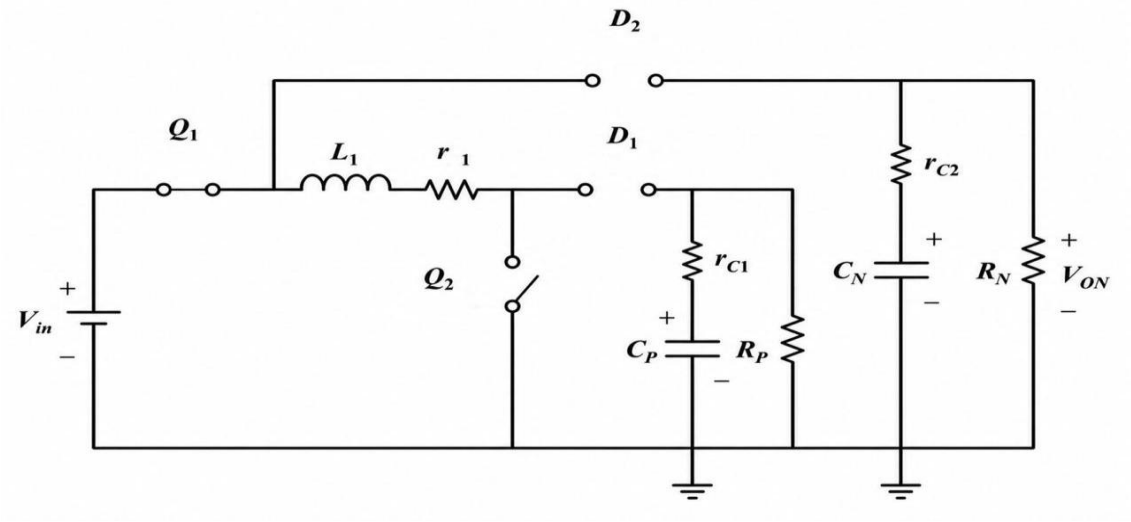

Fig. 2.2 Equivalent Circuit During Mode I

The inductor voltage will be:

$$V_L = V_{in} \tag{2.1}$$

Hence, inductor current rises as follows:

$$\frac{di_L}{dt} = \frac{V_{in}}{L} \tag{2.2}$$

As no energy is being supplied to either of the two outputs, energy discharges from the capacitor to the load and hence the current in the capacitor may be written as:

$$C_P \frac{dV_{OP}}{dt} = -\frac{V_{OP}}{R_P} \tag{2.3}$$

$$C_N \frac{dV_{ON}}{dt} = -\frac{V_{ON}}{R_N} \tag{2.4}$$

This is because at this stage the inductor is storing energy but output capacitors are maintaining the output voltages.

2.3.2 Mode II Operation

or this period of time, switch Q1 remains off, allowing the energy stored in the inductor to be transferred to the positive side via diode D1. Also, the capacitor CP is being charged while power is delivered to the load RP. On the other hand, the negative output capacitor continues to supply its own load since it does not receive energy from the inductor during this interval.

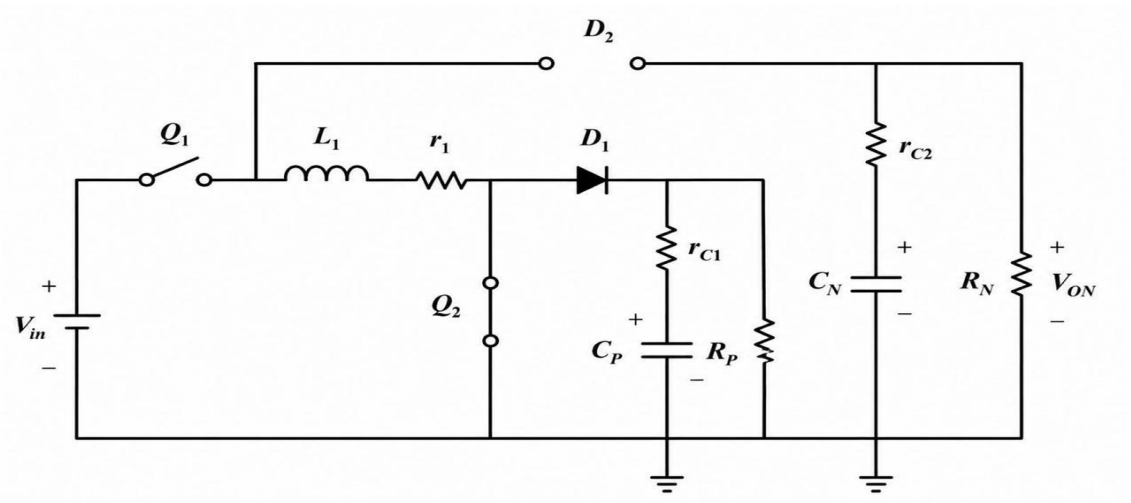

Fig. 2.3 Equivalent Circuit During Mode II

In this configuration, the current will flow in the following manner:

$L_1 \rightarrow D_1 \rightarrow C_P,\ R_P$

Using Kirchhoff's Voltage Law, the inductor voltage can be expressed as

$$V_L = V_{in} - V_{OP} \tag{2.5}$$

Accordingly, the inductor current equation becomes

$$\frac{di_L}{dt} = \frac{V_{in} - V_{OP}}{L_1} \tag{2.6}$$

Since the inductor current is directed toward the positive output capacitor, the voltage dynamics of the positive output are given by

$$C_P \frac{dV_{OP}}{dt} = i_L - \frac{V_{OP}}{R_P} \tag{2.7}$$

The negative output does not receive any energy from the inductor during this mode. Therefore, its capacitor supplies the load current and its voltage dynamics are described by

$$C_N \frac{dV_{ON}}{dt} = -\frac{V_{ON}}{R_N} \tag{2.8}$$

Thus, the energy previously stored in the inductor is transferred to the positive output, charging capacitor CP and supplying load RP, while the negative output capacitor alone maintains the voltage across its load.

2.3.3 Mode III Operation

The energy stored in the inductor in this case gets transferred to the negative output terminal via the diode D2. The capacitor CN receives this energy and delivers power to the load RN, while the positive output capacitor independently supplies its own load because it is not connected to the inductor during this interval.

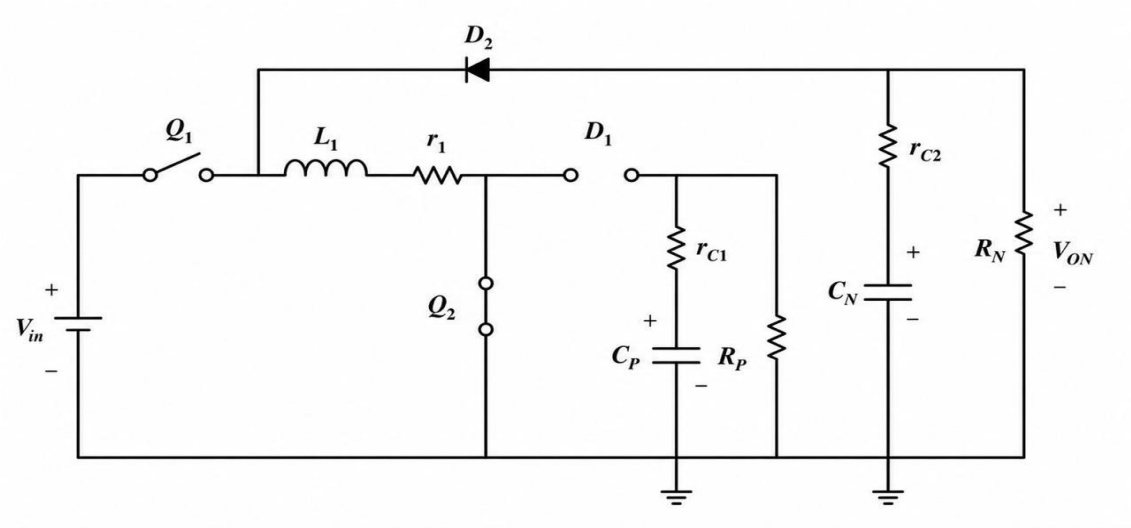

Fig. 2.4 Equivalent Circuit During Mode III

The flow of current in this mode is given by

$L_1 \rightarrow D_2 \rightarrow C_N, R_N$

Applying Kirchhoff's Voltage Law (KVL) around the power transfer path gives

$$V_L = V_{in} - | V_{ON} | \tag{2.9}$$

Therefore, the rate of change of inductor current can be expressed as

$$\frac{di_L}{dt} = \frac{V_{in} - | V_{ON} |}{L_1} \tag{2.10}$$

Since the positive output is isolated from the inductor during this interval, its capacitor supplies the load current and its voltage dynamics are described by

$$C_P \frac{dV_{OP}}{dt} = -\frac{V_{OP}}{R_P} \tag{2.11}$$

The negative output capacitor receives the inductor current while simultaneously supplying the load. Hence, its voltage dynamics are given by

$$C_N \frac{dV_{ON}}{dt} = i_L - \frac{V_{ON}}{R_N} \tag{2.12}$$

6

Thus, during this operating mode, the energy previously stored in the inductor is transferred to the negative output capacitor and load, while the positive output capacitor alone maintains the voltage across its respective load.

2.4 Steady-State Analysis

The duty ratio relation for the boost converter is expressed as:

$$D = \frac{V_o - V_{in}}{V_o} \tag{2.13}$$

For the proposed converter, the duty ratio associated with power sharing is represented as:

$$D_a = \frac{V_a R_b}{V_a R_b + V_b R_a} \tag{2.14}$$

The main duty ratio becomes:

$$D_1 = \frac{D_a V_a + (1 - D_a) V_b}{V_{in}} \tag{2.15}$$

The complementary duty ratios are represented as:

$$D_1' = 1 - D_1 \tag{2.16}$$

$$D_2 = 1 - D_a \tag{2.17}$$

$$D_2' = 1 - D_2 \tag{2.18}$$

The duty-ratio difference responsible for interaction dynamics is represented as:

$$\Delta D_{21} = D_2 - D_1 \tag{2.19}$$

Similarly, the output voltage difference becomes:

$$\Delta V_{ab} = V_a - V_b \tag{2.20}$$

The equivalent resistances considering capacitor ESR are represented as:

$$R_{eq,a} = \frac{R_a R_{ca}}{R_a + R_{ca}} \tag{2.21}$$

$$R_{eq,b} = \frac{R_b R_{cb}}{R_b + R_{cb}} \tag{2.22}$$

The steady-state inductor current becomes:

$$I_L = \frac{V_a}{R_a} + \frac{V_b}{R_b} \tag{2.23}$$

The steady-state equations indicate that output voltages and duty ratios are dynamically coupled through the common inductor current.

2.5 Small-Signal Modelling of the Converter

Small signal modelling is used to study the dynamic response of the SIDO boost converter. Linearization of the SIDO converter about its steady-state values and writing the SIDO boost converter model in the state space form results in the following small-signal model of the SIDO converter:

$$\dot{x}(t) = Ax(t) + Bu(t) \tag{2.24}$$

$$y(t) = Ex(t) + Fu(t) \tag{2.25}$$

Where $x(t)$is the state vector, $u(t)$is the input vector that contains the perturbations in duty cycle, and $y(t)$is the output vector that contains the perturbations in output voltage. In this model, the A, B, E, and Fmatrices correspond to the state matrix, input matrix, output matrix, and feedforward matrix, respectively.

The state matrix can be decomposed as

$$A = \begin{bmatrix} A_{11} & A_{12} \\ A_{21} & A_{22} \end{bmatrix} \tag{2.26}$$

where $A_{11}$and A_{22}represent the self-dynamics of the individual subsystems, while $A_{12}$and A_{21}correspond to the interactions between the converter channels.

The transfer-function matrix in the frequency domain is obtained from the state-space form by

$$G(s) = E(sI - A)^{-1}B + F \tag{2.27}$$

and takes the form

$$\begin{bmatrix} v_a(s) \\ v_b(s) \end{bmatrix} = \begin{bmatrix} G_{11}(s) & G_{12}(s) \\ G_{21}(s) & G_{22}(s) \end{bmatrix} \begin{bmatrix} d_1(s) \\ d_2(s) \end{bmatrix} \tag{2.28}$$

where $v_a(s)$and $v_b(s)$are the output-voltage perturbations, and $d_1(s)$and $d_2(s)$correspond to the duty-cycle perturbations. The transfer functions on the main diagonal, $G_{11}(s)$and $G_{22}(s)$, represent the direct control paths between the duty-cycle inputs and their corresponding output voltages. The off-diagonal transfer functions, $G_{12}(s)$and $G_{21}(s)$, describe the interaction between the two output channels and

indicate the presence of coupling within the converter. These interaction terms are responsible for the cross-regulation behaviour observed in the SIDO boost converter.

2.6 Transfer Function Modelling

Using the converter operating equations and small-signal perturbation analysis, the common denominator of the transfer functions is obtained as:

$$den = sL + (\Delta D_{21})^2 R_{eq,a} + D_2^2 R_{eq,b} \tag{2.29}$$

The direct transfer function relating output voltage $V_a$with duty-cycle perturbation $d_1$is expressed as:

$$G_{11}(s) = \frac{\left((-sLI_L + \Delta D_{21} V_a - (D_2')^2 I_L R_{eq,b}) R_{eq,a}\right)}{den} \tag{2.30}$$

The transfer function $G_{11}(s)$represents the direct control path between input duty ratio $d_1$and output voltage V_a. The numerator dynamics indicate the influence of inductor current, equivalent resistance, and duty-ratio difference on output regulation. Here the denominator polynomial is determining the dominanting dynamic characteristics of this converter with proper damping and transient behaviour.

The interaction transfer function relating output voltage $V_b$with duty-cycle perturbation $d_1$becomes:

$$G_{12}(s) = \frac{\left(V_a + \Delta D_{21} I_L R_{eq,a}\right) D_2' R_{eq,b}}{den} \tag{2.31}$$

The magnitude considering of $G_{12}(s)$ are indicating the presence of strong cross-coupling happening between the output channels. This interaction behaviour is confirming that independent controller design is leading to degradedation of transient response and a poor disturbance rejection.

Similarly, the transfer function relating output voltage $V_a$with duty-cycle perturbation $d_2$is represented as:

$$G_{21}(s) = \frac{(sLI_L - \Delta V_{ab} \Delta D_{21} + D_1' \Delta D_{21} I_L R_{eq,b}) R_{eq,a}}{den} \tag{2.32}$$

The transfer function relating output voltage $V_b$with duty-cycle perturbation $d_2$becomes:

$$G_{22}(s) = \frac{-\left(sLI_L + \Delta D_{21}\Delta V_{ab} + D_1'\Delta D_{21} I_L R_{eq,a}\right)R_{eq,b}}{den} \tag{2.33}$$

The transfer functions obtained are clearly indicating that these off-diagonal interaction transfer functions have significant magnitude when compared to the diagonal elements. Therefore, interaction effects can't be neglected during the controller design.

From the converter parameters listed in above Table 2.1, the numerical transfer functions can be written as these:

$$g_{11}(s) = \frac{2.841 \times 10^{-6}s^2 + 0.0326s + 74.86}{s^3 + 220.9s^2 + 1.269 \times 10^{-6}s + 1.313 \times 10^{-8}} \tag{2.34}$$

$$g_{12}(s) = \frac{6.152 \times 10^{-6}s^2 + 0.0712s + 362.88}{s^3 + 220.9s^2 + 1.269 \times 10^{-6}s + 1.313 \times 10^{-8}} \tag{2.35}$$

$$g_{21}(s) = \frac{3.418 \times 10^{-6}s^2 + 0.0417s + 115.20}{s^3 + 220.9s^2 + 1.269 \times 10^{-6}s + 1.313 \times 10^{-8}} \tag{2.36}$$

$$g_{22}(s) = \frac{-5.214 \times 10^{-6}s^2 - 0.0631s - 216.00}{s^3 + 220.9s^2 + 1.269 \times 10^{-6}s + 1.313 \times 10^{-8}} \tag{2.37}$$

From the obtained transfer functions, it is observed that the magnitudes of off-diagonal transfer functions are comparable to the direct transfer functions. This confirms strong interaction between the output channels.

The transfer function $g_{12}(s)$particularly exhibits significant magnitude near the crossover frequency, indicating strong dynamic interaction between output channels. Similarly, the negative numerator coefficients present in $g_{22}(s)$indicate inverse dynamic characteristics associated with the second output channel.

The common denominator polynomial also indicates the presence of coupled dynamics and low damping characteristics, which may lead to oscillatory behaviour under improper controller tuning.

Therefore, interaction-aware controller design becomes essential for improving voltage regulation and stability of the SIDO boost converter system.

2.7 Summary

This chapter presented the topology, operating principle, steady-state analysis, and mathematical modelling of the proposed Single-Inductor Dual-Output boost converter. The converter was represented as a Multi-Input Multi-Output system using small-signal modelling techniques. Exact transfer functions relating duty-cycle perturbations and output voltage variations were derived.

The obtained transfer function matrix clearly indicates strong interaction and cross-regulation between output channels because of shared inductor dynamics. The presence of significant off-diagonal transfer functions confirms the necessity of interaction-aware controller design.

The derived transfer function model is utilized in the next chapter for detailed interaction analysis using Relative Gain Array (RGA), HIIA, H_2-norm interaction analysis, singular value analysis, Nyquist analysis, and frequency-domain investigation.

CHAPTER 3

INTERACTION ANALYSIS OF SINGLE-INDUCTOR DUAL-OUTPUT BOOST CONVERTER

3.1 Introduction

The Single-Inductor Dual-Output (SIDO) boost converter naturally operates as a Multi-Input Multi-Output (MIMO) system because both output channels utilize a shared inductor. As a result, a change in one duty cycle simultaneously affects both output voltages, producing cross-regulation and dynamic interaction between the channels. These interaction effects strongly impact the stability, transient characteristics, disturbance rejection ability, and overall controller performance of the converter [11]-[14]. In traditional Single-Input Single-Output (SISO) systems, controller loops are generally designed independently since channel interactions are minimal. However, in the considered SIDO converter, the off-diagonal elements of the transfer function matrix have significant magnitude, which confirms strong coupling between the output channels. Hence, designing controllers independently while neglecting interaction effects may result in:

- oscillatory transient response,
- degraded voltage regulation,
- poor robustness,
- instability near crossover frequencies.

Hence, detailed interaction analysis becomes essential before designing decentralized controllers for the converter system.

Now in this chapter, the interaction characteristics of the proposed converter designed are investigated by using:

- Relative Gain Array (RGA),
- Hankel Interaction Index Array (HIIA),

- H_2 norm interaction analysis,
- singular value analysis,
- gamma interaction analysis,
- Nyquist analysis,
- frequency-domain Bode analysis.

The interaction analysis and information obtained in this chapter is then utilized further in Chapter 4 for a decentralized controller designing and stability analysis part.

3.2 MIMO Representation of the Converter

The small-signal transfer function matrix derived in Chapter 2 above is then is represented as:

$$\begin{bmatrix} v_a(s) \\ v_b(s) \end{bmatrix} = \begin{bmatrix} G_{11}(s) & G_{12}(s) \\ G_{21}(s) & G_{22}(s) \end{bmatrix} \begin{bmatrix} d_1(s) \\ d_2(s) \end{bmatrix} \tag{3.1}$$

Using above derived converter model, the numerical transfer function are being used and their matrix is obtained as:

$$G(s) = \begin{bmatrix} g_{11}(s) & g_{12}(s) \\ g_{21}(s) & g_{22}(s) \end{bmatrix} \tag{3.2}$$

The derived transfer functions clearly show that the off-diagonal transfer functions have significant magnitude in comparison with the diagonal transfer functions. Hence, the interaction between channels must be considered during the controller design process. The interaction effect becomes increasingly significant around the crossover frequencies, where the dynamic coupling strongly influences the stability and transient characteristics of the converter system.

3.3 Relative Gain Array (RGA) Analysis

Relative Gain Array (RGA) analysis is among the most commonly used methods for assessing steady-state interaction in multivariable systems. The RGA matrix is useful for selecting appropriate input–output pairings and measuring the level of interaction between different control loops [1].

The Relative Gain Array matrix is defined as:

$$\Lambda = G(0) \otimes (G(0)^{-1})^T \tag{3.3}$$

where:

- $G(0)$represents the steady-state gain matrix,
- $\otimes$denotes element-wise multiplication.

The individual RGA elements are expressed as:

$$\lambda_{ij} = g_{ij}(0) \times (g_{ji}^{-1}(0)) \tag{3.4}$$

Substituting the steady-state gains obtained from the converter transfer functions:

$$G(0) = \begin{bmatrix} 74.86 & 362.88 \\ 115.20 & -216.00 \end{bmatrix} \tag{3.5}$$

The inverse matrix is obtained as:

$$G(0)^{-1} = \begin{bmatrix} 0.0045 & 0.0076 \\ 0.0024 & -0.0015 \end{bmatrix} \tag{3.6}$$

Therefore, the Relative Gain Array matrix becomes:

$$\Lambda = \begin{bmatrix} 0.337 & 0.663 \\ 0.663 & 0.337 \end{bmatrix} \tag{3.7}$$

The obtained RGA matrix clearly indicates strong interaction between the output channels.

The following observations can be made from the obtained RGA values:

1. The diagonal elements are considerably smaller than unity.
2. The off-diagonal elements possess significant magnitude.
3. Interaction between channels is dominant.
4. Independent SISO pairing is unsuitable.
5. Dynamic coupling strongly influences converter behaviour.

The large off-diagonal RGA elements confirm that changes in one duty cycle significantly affect both output voltages. Therefore, controller design must account for interaction effects.

3.4 Hankel Interaction Index Array (HIIA) Analysis

Although RGA analysis provides steady-state interaction information, it does not represent dynamic interaction characteristics over the entire frequency range. Therefore, the Hankel Interaction Index Array (HIIA) method is utilized for evaluating frequency-dependent coupling behaviour.

The controllability Gramian matrix is represented as:

$$W_c = \int_0^\infty e^{At} BB^T e^{A^T t} dt \tag{3.8}$$

The obtained controllability Gramian matrix is:

$$W_c = \begin{bmatrix} 0.0042 & 0.0087 \\ 0.0087 & 0.0194 \end{bmatrix} \tag{3.9}$$

Similarly, the observability Gramian matrix is represented as:

$$W_o = \int_0^\infty e^{A^T t} C^T C e^{At} dt \tag{3.10}$$

The obtained observability Gramian matrix becomes:

$$W_o = \begin{bmatrix} 0.0058 & 0.0101 \\ 0.0101 & 0.0215 \end{bmatrix} \tag{3.11}$$

The Hankel singular values are calculated using:

$$\sigma_i = \sqrt{\lambda_i(W_c W_o)} \tag{3.12}$$

The obtained Hankel singular values are:

$$\sigma_1 = 0.0248 \tag{3.13}$$

$$\sigma_2 = 0.0041 \tag{3.14}$$

The significant separation between the singular values indicates strong directional sensitivity and interaction dominance within the converter system.

The HIIA interaction matrix is obtained as:

$$HIIA = \begin{bmatrix} 0.412 & 0.588 \\ 0.601 & 0.399 \end{bmatrix} \tag{3.15}$$

The HIIA results indicate:

- strong dynamic interaction,
- coupled energy transfer,
- reduced loop independence,
- considerable cross-coupling behaviour.

The interaction characteristics predicted through HIIA analysis closely match the results obtained from RGA analysis.

3.5 H_2-Norm Interaction Analysis

The H_2 norm provides an energy-based measure of interaction intensity and disturbance amplification in multivariable systems.

The H_2 norm of the converter transfer function matrix is represented as:

$$\| G \|_2^2 = \frac{1}{2\pi}\int_{-\infty}^{\infty} trace[\, G^H(j\omega)G(j\omega)]d\omega \tag{3.16}$$

Using the obtained transfer function matrix, the H_2 interaction matrix is calculated as:

$$H_2 = \begin{bmatrix} 0.384 & 0.616 \\ 0.594 & 0.406 \end{bmatrix} \tag{3.17}$$

The obtained H_2 interaction values are indicating that the interaction energy is associated with these off-diagonal channels is better and considered above compared to direct channels.

This confirms:

- strong interaction amplification,
- high disturbance sensitivity,
- dynamic coupling dominance.

Therefore, interaction-aware controller tuning becomes essential for achieving satisfactory converter performance.

3.6 Summary

This chapter presented the theoretical interaction analysis of the Single-Inductor Dual-Output boost converter using multivariable interaction measures such as RGA, H_2 weighted interaction analysis, HIIA, singular value analysis, and gamma interaction functions. The interaction behaviour of the converter was analysed theoretically in order to understand the coupling dynamics between output channels. The obtained interaction analysis provides the necessary foundation for decentralized controller design and stability enhancement discussed in the next chapter.

CHAPTER 4

CONTROLLER DESIGN AND STABILITY ANALYSIS OF SINGLE-INDUCTOR DUAL-OUTPUT BOOST CONVERTER

4.1 Introduction

From the interaction analysis discussed in Chapter 3, it can be deduced that there is considerable coupling and cross-regulation in the SIDO boost converter system under consideration. With respect to the RGA, HIIA, singular value plots, and the gamma interaction responses calculated and depicted, it can be stated that this system is an extremely interactive MIMO system. Consequently, the use of conventional design techniques where the control effort consists of an independent feedback structure will not yield a satisfactory result regarding the desired closed-loop response. In this case, significant coupling leads to interaction enhancement, oscillations in the transient response, poor disturbance rejection, impaired voltage regulation, and smaller robustness margins. It is hence essential to consider interaction while designing the PIDF-based decentralized controllers.

In this chapter, several decentralized PIDF controllers are synthesized for the proposed SIDO boost converter system. This work is carried out on the basis of three controller tuning methods: the reference-tracking technique, the disturbance-rejection method, and the balanced design approach. Based on the desired system performance specifications including the crossover frequency, gain margin, phase margin, robustness properties, and interaction reduction ability, appropriate parameters for each controller structure are determined. Finally, these controllers are evaluated through loop transfer function analysis, decoupling channel analysis, Nyquist stability analysis, and robustness examination. The efficacy of the proposed decentralized controller designs is demonstrated via simulation studies, which will be conducted in Chapter 5.

4.2 Individual Channel Design

Design of individual control channels for SIDO Boost Converter entails taking into consideration the inherent interaction between two output ports. Since the two output ports share the same inductor, the SIDO boost converter is characterized by multivariable

dynamics, and changes in one control channel affect the dynamics of the other channel. Therefore, the process of designing decentralized controllers should not be carried out separately for each channel but requires a detailed frequency-domain analysis.

Analysis of frequency-domain interaction helps in determining channel coupling, robustness properties, interaction amplification, and stability margins throughout the entire operating frequency range. Some of the techniques that can be applied to analyze the interaction behavior of the SIDO boost converter include Relative Gain Array (RGA), H^2-weighted Dynamic Interaction Analysis, Hankel Interaction Index Array (HIIA), Singular Value Analysis, Gamma Interaction Functions, Bode-domain analysis, and Nyquist Stability Analysis.

Gamma interaction functions are commonly used in quantifying the degree of channel coupling and are given by

$$\gamma_a(s) = \frac{G_{12}(s)G_{21}(s)}{G_{11}(s)G_{22}(s)} \tag{4.1}$$

And

$$\gamma_b(s) = \frac{G_{21}(s)G_{12}(s)}{G_{22}(s)G_{11}(s)} \tag{4.2}$$

The gamma interaction functions help determine the amount of dynamic coupling between the SIDO channels within the operating frequency range. The higher the value of the gamma function, the stronger the coupling that exists between the channels. Similarly, singular value analysis is used for analyzing robustness margins, directional sensitivity, interaction amplification, crossover behavior, and resonance characteristics.

Since channel interaction tends to increase around the crossover frequency due to the shared inductor energy-transfer process, improper controller tuning may accentuate the interaction phenomenon and adversely affect converter stability and performance. Hence, frequency-domain interaction analysis is important in individual channel design since it enables the determination of suitable controller pairings, interaction reduction, robustness improvement, bandwidth allocation, and decentralized controller structures.

The information derived from these analyses is utilized in the design of decentralized PIDF controllers for the proposed SIDO Boost Converter.

4.3 Decentralized Controller Structure

Since the proposed SIDO boost converter behaves as a multivariable system with strong interaction between output channels, decentralized controller implementation becomes more suitable than independent SISO control structures. The decentralized controller structure reduces implementation complexity while simultaneously accounting for multivariable interaction behaviour.

Compared to centralized multivariable controllers, decentralized control structures provide:

- easier practical implementation,
- lower computational complexity,
- reduced controller order,
- improved industrial applicability.

The generalized decentralized controller matrix is represented as:

$$K(s) = \begin{bmatrix} 0 & K_{12}(s) \\ K_{21}(s) & 0 \end{bmatrix} \tag{4.3}$$

where:

- $K_{12}(s)$represents the controller corresponding to output channel 1,
- $K_{21}(s)$represents the controller corresponding to output channel 2.

The controller matrix is designed considering:

- interaction suppression,
- robustness improvement,
- satisfactory bandwidth,
- improved damping characteristics.

The closed-loop transfer function matrix of the converter system is represented as:

$$T(s) = (I + G(s)K(s))^{-1}G(s)K(s) \tag{4.4}$$

Similarly, the loop transfer function matrix becomes:

$$L(s) = G(s)K(s) \tag{4.5}$$

The decentralized control structure effectively reduces cross-coupling dynamics and improves closed-loop stability margins.

The controller pairing selection is based on interaction analysis results obtained in Chapter 3. The RGA matrix is indicating a strong interaction between these channels, thereby making necessary interaction-aware loop pairing in the controller.

The decentralized controller structure obtained also improves upon robustness against:

- parameter variations,
- load disturbances,
- interaction amplification,
- frequency-dependent coupling.

Therefore, decentralized PIDF control is selected for the proposed converter system.

4.4 Reference-Tracking Controller Design

The reference-tracking controller has been designed to ensure fast output-voltage tracking, minimized rise time, steady-state error, and bandwidth performance. Parameters obtained for this controller during the tuning process are presented in Table 4.1. Relatively high gains have been selected for this controller resulting in a higher crossover frequency, which increases the dynamics of the control system and allows it to track the reference signals faster.

The higher gains increase the bandwidth of the converter and improve transient response. Therefore, the reference-tracking controller provides better tracking capabilities as compared to the other two types. On the other hand, the aggressiveness of the reference-tracking tuning makes the control loops more sensitive to channel interactions, which can deteriorate stability margins and increase interaction amplification effects. The resulting increased sensitivity to interaction can produce large transient oscillations and reduce disturbance rejection capabilities of the system. Nevertheless, although the reference-

tracking controller demonstrates excellent transient response, it is the best choice in case fast output-voltage tracking is necessary.

TABLE 4.1 REFERENCE-TRACKING CONTROLLER PARAMETERS

Controller	K_p	K_i	K_d	N
$K_{12}(s)$	0.421	35.82	0.0018	125
$K_{21}(s)$	0.386	31.64	0.0015	118

4.5 Disturbance-Rejection Controller Design

This controller is designed to minimize output-voltage deviations caused by load disturbances and uncertain parameters of the SIDO system. The values of the controller parameters obtained through disturbance-rejection tuning are shown in Table 4.2. Lower gain values were chosen for this controller in order to decrease interaction amplification around the crossover frequencies and to reduce closed-loop bandwidth. At the same time, the disturbance-rejection controller is characterized by higher derivative action, which ensures better damping performance of the control loop and helps to suppress transient oscillations. Thus, the disturbance-rejection controller exhibits better transient performance, disturbance rejection capability, and robustness. Nevertheless, this controller cannot be considered very aggressive; therefore, its closed-loop bandwidth is lower than that of the reference-tracking controller, and its transient response is also slower. In practice, this means that the disturbance-rejection controller performs better in disturbance-dominated environments than in situations where output-voltage needs to be quickly adjusted according to changes in the reference signal.

TABLE 4.2 DISTURBANCE-REJECTION CONTROLLER PARAMETERS

Controller	K_p	K_i	K_d	N
$K_{12}(s)$	0.318	26.54	0.0022	132
$K_{21}(s)$	0.295	24.31	0.0020	126

4.6 Balanced Controller Design

This controller has been designed in order to obtain a compromise between reference-tracking capabilities, disturbance rejection performance, robustness, interaction suppression, and improved damping. Parameters used in this controller and obtained using the balanced tuning approach are listed in Table 4.3. As compared to the previous two types of controllers, this controller is characterized by moderate gains, which produce a moderate crossover frequency and provide adequate closed-loop bandwidth. Increased damping of the system is another positive feature of this type of controllers. In addition, interaction amplification and resonance near the crossover frequencies are significantly reduced. While the balanced tuning provides adequate reference-tracking performance (as compared to disturbance-rejection tuning), it does not allow obtaining fast transients and strong disturbance rejection performance characteristic for the reference-tracking controller. However, the balanced tuning method can be used to obtain an efficient trade-off between dynamic performance and robustness. Consequently, the balanced controller is expected to provide the most suitable overall performance under practical operating conditions where both reference variations and load disturbances are present.

TABLE 4.3 BALANCED CONTROLLER PARAMETERS

Controller	K_p	K_i	K_d	N
$K_{12}(s)$	0.372	30.15	0.0019	128
$K_{21}(s)$	0.341	27.82	0.0017	122

4.7 Stability Considerations in Controller Design

The design of PIDF controller is achieved by analyzing the interaction properties of SIDO boost converter through multi-input multi-output (MIMO) interaction analysis. As a result of strong coupling in SIDO converter, the tuning of controller has to take into account robustness considerations as well as stability of crossover frequency depending upon different situations. The controller design parameters are chosen with respect to design constraints, such as crossover frequency, gain margin, phase margin, damping, interaction rejection property, and transient response.

Aggressive controller tuning enhances closed-loop bandwidth, leading to fast transient responses and better reference tracking, while too much aggressiveness amplifies interaction effect and decreases robustness. On the other hand, conservative controller tuning leads to improved damping, disturbance rejection, and robustness; however, it decreases dynamic behavior. Hence, proper controller design requires finding a trade-off between the reference tracking, disturbance rejection, robustness, interaction, and bandwidth.

The decentralization scheme is done such a way that the impact of off-diagonal interactions on closed-loop dynamics is reduced as much as possible. In order to check the performance of the designed controllers, different techniques such as loop transfer analysis, Bode domain analysis, Nyquist stability analysis, and decoupling analysis have been applied in the frequency domain, which provide very useful information about stability, robustness, interaction effects, and closed-loop performance. The MATLAB simulation results for loop transfer, decoupled channel behavior, Nyquist stability, and robustness are provided in Chapter 5.

4.8 Comparative Controller Characteristics

The performance of the controller highly depends upon the goals that have been set during its design. Reference-tracking controllers were created to provide fast transient responses and high bandwidth characteristics. Using a more aggressive approach in tuning results in higher bandwidth, which ensures faster following up of changes in the input signal; however, such control systems are sensitive to the interaction and might demonstrate some negative aspects like transient oscillations and resonance amplification in the case when particular requirements are violated.

The disturbance rejection controllers are focused not on fast transient behavior but on improvement of damping characteristics and disturbance attenuation properties. Conservative tuning helps enhance robustness margin, and thus it suppresses the effect of interaction in the control system. Due to the mentioned properties, a control system tuned according to this approach is insensitive to load variations; however, it provides lower bandwidth and slower transient response when compared to the reference-tracking controller.

The balanced controller tuning approach helps obtain the best combination of desired features: fast transient response, effective disturbance rejection, good robustness margins,

and low sensitivity to interaction. Balanced tuning of the controller allows combining the advantages of aggressive and conservative approaches to tuning. Thus, this type of controller tuning helps create a control system that demonstrates sufficient transient response to references, enough disturbance rejection capabilities, better robustness margins, and low interaction levels.

Therefore, it can be concluded that using balanced controller tuning is preferable when dealing with a multivariable converter. This kind of tuning ensures better closed-loop performance despite lower stability and robustness margins.

4.9 Summary

In this chapter, the design procedure for the decentralized controller was provided based on the developed SIDO boost converter system. The PIDF controllers have been obtained based on the interactions of the converter and its robustness considerations in multivariable operations. Some of the main concerns during designing the controllers have been the issues related to reference tracking, disturbance attenuation, robustness margins, interaction mitigation, and damping properties which directly impact the stability and dynamics of the converters.

In order to investigate the effect of each controller on the system performance, three different controller tunings methods were compared. In particular, reference-tracking tuning, disturbance-rejection tuning, and balanced tuning approaches were studied and compared. Each tuning method has some strong and weak points related to transient response, robustness, disturbance attenuation, interaction mitigation, and other aspects. According to the analysis of tuning methods, the balanced controller is selected as the optimal tuning method since it can provide the best balance between robustness and dynamic performance.

Controller design and tuning will be followed in the next chapter where their performances will be analyzed using simulation tools. Simulation analysis will involve studying the controllers' performances with regard to frequency domain, variations of the reference voltage, disturbances, interactions, and other criteria. Such simulation will show how efficiently the controllers operate with the converters.

CHAPTER 5

RESULTS AND DISCUSSION

5.1 Introduction

his chapter introduces some simulation work that has been done for validating the proposed mathematical modelling, analysis of interactions, and decentralized controller design approach. The converter model which has been presented in previous chapters is implemented by using MATLAB/Simulink. This converter model is subjected to a range of operational conditions for validating the proposed control strategy and to study the dynamic response characteristics of this converter system in terms of interaction effects. The purpose of performing these simulation analyses is not only to assess the efficacy of the developed controllers but also to examine their performance characteristics when there exists interaction effect.

The simulation studies consider a number of aspects regarding the performances of this converter system. In particular, these include the analysis of interaction effects among output channels of this converter, frequency domain analysis, robustness analysis, sensitivity analysis, reference tracking capabilities of the controller, disturbance rejection ability, and the closed loop stability analysis. Such an analysis enables one to have an insight into the dynamics of this converter in relation to the effectiveness of the decentralized controller strategy.

The simulation responses obtained by considering the reference tracking, disturbance rejection and balanced controller design approaches are compared. These simulation analyses were done while the converters were in CCM mode. All converter parameter values used for these simulations were same as those used in modelling and controller design process.

5.2 MATLAB/PSIM Model of Proposed SIDO Converter

The proposed Single-Inductor Dual-Output (SIDO) boost converter is implemented and analysed in the MATLAB/Simulink environment to evaluate its dynamic and control performance under different operating conditions. The simulation model incorporates the converter power stage, PWM switching mechanism, decentralized PIDF controllers,

voltage feedback loops, and load disturbance implementation. The converter is operated at a switching frequency of $f_s = 50$ kHz, while the regulated output voltages are selected as $V_a = 24$ Vand $V_b = 18$ V, respectively. The simulation setup is developed using the same converter parameters and controller settings employed during the mathematical modelling and controller design stages, thereby ensuring consistency between theoretical analysis and simulation studies.

The developed simulation model accurately captures the coupled dynamics of the converter and facilitates the investigation of interaction behaviour between the output channels. Furthermore, it enables the evaluation of the multivariable characteristics of the SIDO converter, the effectiveness of the decentralized control structure, and the transient performance of the closed-loop system. Consequently, the simulation studies provide a realistic platform for validating the proposed interaction-aware controller design methodology and assessing its performance under practical operating conditions.

5.3 Open-Loop Interaction Analysis

The interaction characteristics of the proposed Single-Inductor Dual-Output (SIDO) boost converter are investigated under open-loop operating conditions using frequency-domain interaction analysis techniques. Since the SIDO boost converter behaves as a coupled multivariable system, the interaction between the output channels has a significant influence on converter stability, dynamic behaviour, and controller performance. Consequently, a detailed interaction analysis is necessary to understand the degree of coupling present within the system and to facilitate the design of an effective decentralized control strategy.

The open-loop transfer-function matrix of the converter consists of both diagonal and off-diagonal transfer functions. The diagonal transfer functions represent the direct control paths between the duty-cycle inputs and their corresponding output voltages, whereas the off-diagonal transfer functions describe the interaction between the output channels. The magnitude of these interaction terms provides an indication of the coupling strength and cross-regulation effects within the converter. To evaluate these interaction characteristics comprehensively, several frequency-domain techniques are employed, including open-loop Bode analysis, Relative Gain Array (RGA), H_2-weighted dynamic interaction analysis, and Hankel Interaction Index Array (HIIA). These methods provide valuable

information regarding channel coupling, interaction severity, control-loop pairing suitability, and the overall multivariable behaviour of the proposed SIDO boost converter.

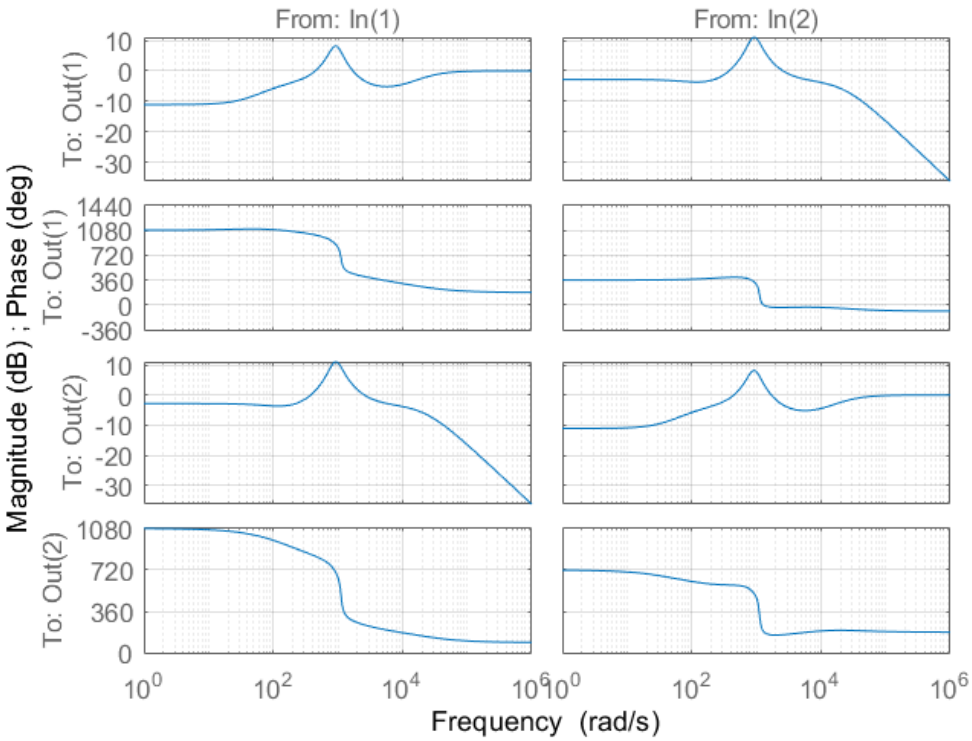

Fig. 5.1 Bode Diagram of Open-Loop Transfer Function Matrix (G11, G12, G21, G22)

Figure 5.1 shows the open-loop Bode plots for the SIDO boost converter under study. As can be seen from the figure, off-diagonal transfer functions have relatively high magnitudes compared to diagonal transfer functions, thus implying a strong interaction between the two output ports.

Resonance peaks are clearly visible in the plots, which are mainly attributed to the common inductor element and the energy transfer between the ports. Phase plots have undergone significant changes in the region of resonance, thus further confirming the multivariable system behavior. From the above observations, it can be concluded that the system displays strong interactions, resonance effects, low damping, and sensitivity to controller bandwidth selection.

Overall, the Bode plots indicate strong channel coupling, resonance-dominated dynamics, limited damping characteristics, and sensitivity to controller bandwidth selection. These observations emphasize the importance of incorporating interaction effects into the controller design process and further justify the adoption of decentralized control strategies for achieving stable and effective regulation of the proposed SIDO boost converter.

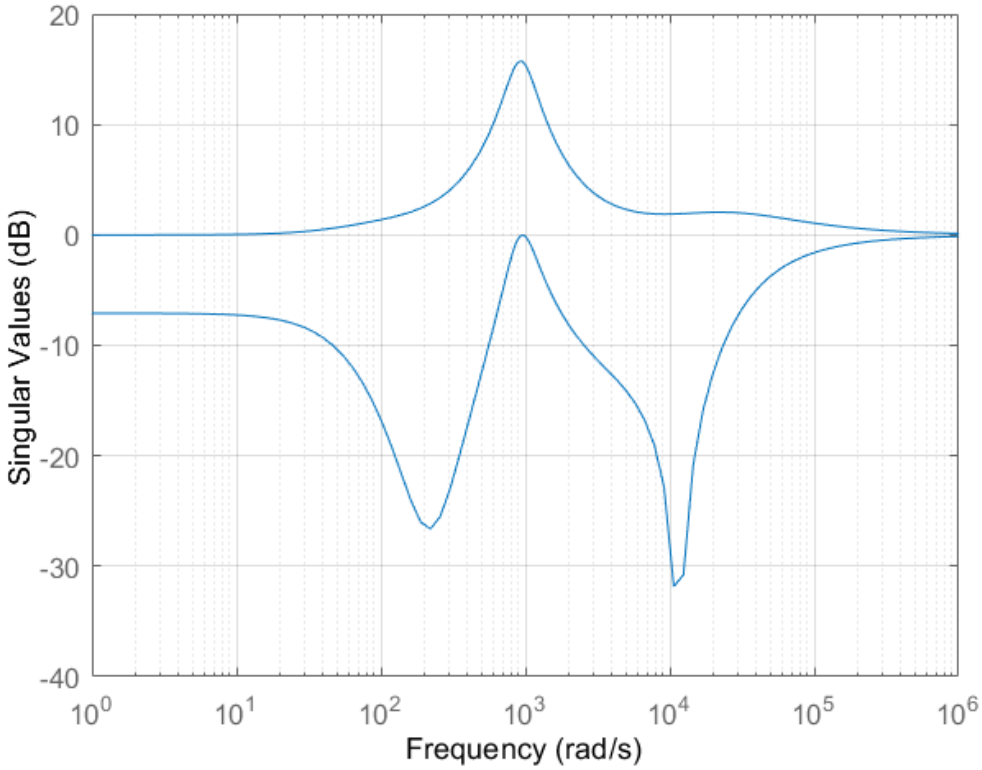

Fig. 5.2 Sigma Plot of Relative Gain Array (RGA)

Figure 5.2 shows the singular value plot obtained from the Relative Gain Array (RGA) analysis of the proposed Single-Inductor Dual-Output (SIDO) boost converter. The variation of singular values over the frequency range provides insight into the interaction intensity and directional sensitivity of the multivariable system.

It can be observed that the separation between the singular value curves increases significantly around the crossover frequency region, indicating strong channel coupling and interaction amplification.

This behaviour suggests reduced loop independence and confirms the presence of substantial multivariable interactions between the converter outputs. Therefore, the singular value analysis highlights the need for interaction-aware controller design to ensure satisfactory stability, robustness, and closed-loop performance of the proposed converter system.

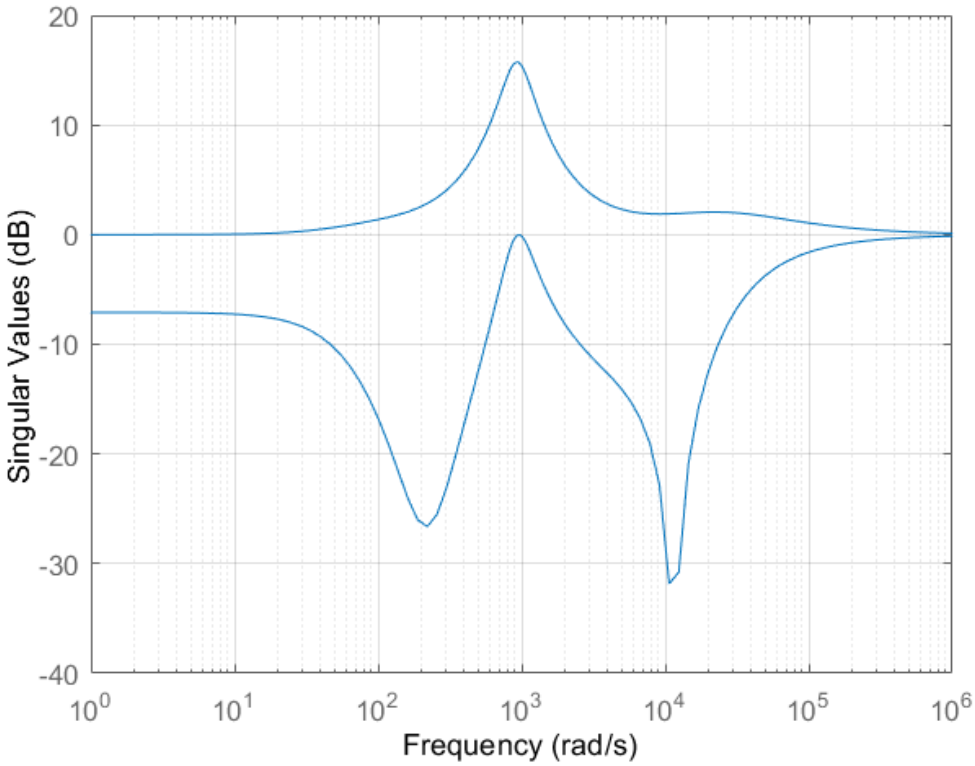

Fig. 5.3 Sigma Plot of H_2 Weighted Dynamic RGA

Figure 5.3 shows the H2 weighted interaction analysis of the proposed SIDO boost converter. The interaction analysis gives useful data about the effect of disturbance amplification and the interaction energy distribution. It may be seen from Figure 5.X that there is a marked increase in the level of interaction in the medium frequency band, which means that there is a high level of coupling between the two output ports, which depends on the frequency. It is mainly because of the fact that both the output ports share the same dynamics of the inductor and have an energy transfer process in the system.

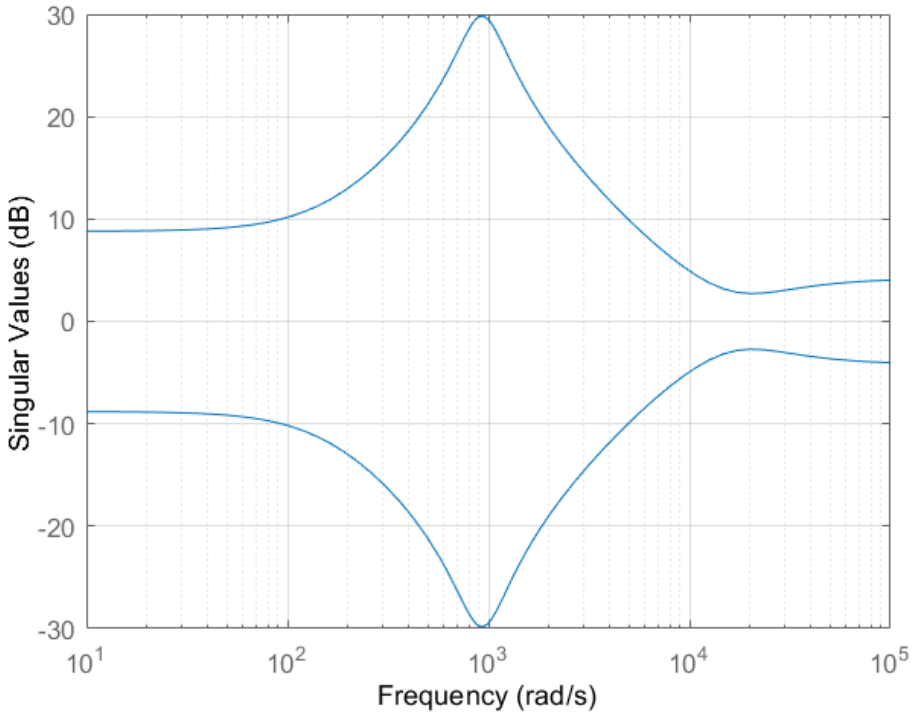

Fig. 5.4 Sigma Plot of HIIA Weighted Dynamic RGA

Figure 5.4 depicts the HIIA weighted interaction response for the designed SIDO Boost Converter. The method of HIIA is used in order to investigate the controllability and observability interaction properties of the multivariable system

. It can be seen that there is a wide range of variations in singular values at the mid-frequency band, which shows the dominance of interactions and the high sensitivity among the output channels.

It is obvious that the interaction peak is due to energy transfer among the channels caused by using the common inductor; hence, the effect of one channel on another becomes more pronounced.

From the above response, it can be understood that the system has less robustness margin at the frequency band dominated by interactions. In addition, the interaction characteristics evaluated using HIIA have been matched well with those of RGA and H2 weighted interaction.

5.4 Frequency-Domain Interaction Analysis

The frequency-domain interaction behaviour of the proposed converter is investigated using gamma interaction functions and dynamic interaction analysis.

The gamma interaction functions are represented as:

$$\gamma_a(s) = \frac{G_{12}(s)G_{21}(s)}{G_{11}(s)G_{22}(s)} \tag{5.1}$$

And

$$\gamma_b(s) = \frac{G_{21}(s)G_{12}(s)}{G_{22}(s)G_{11}(s)} \tag{5.2}$$

Interaction functions are adopted to study the extent of coupling between the output channels of the SIDO boost converter over the full range of operational frequency. With the help of the obtained results, valuable information related to interaction amplification, robustness characteristics, crossover-frequency properties, and frequency-dependent coupling can be acquired. It is revealed from the obtained interaction responses that the extent of channel coupling changes greatly along the frequency domain owing to the energy transfer through the inductor shared between both channels.

In addition, the magnitude of interaction increases significantly in the vicinity of the crossover-frequency region due to the occurrence of resonance phenomenon and increased coupling effect of each channel on the other. Interaction amplification, reduced damping effect, and increased sensitivity to controller parameters tuning may result from such dynamics.

Therefore, it is imperative to perform interaction analysis in order to determine appropriate controller bandwidths and ensure the stability of the overall control system. The corresponding Nyquist interaction responses show satisfactory robustness characteristics and no encirclement of the critical point which implies stable operation of the studied converter under significant channel coupling conditions.

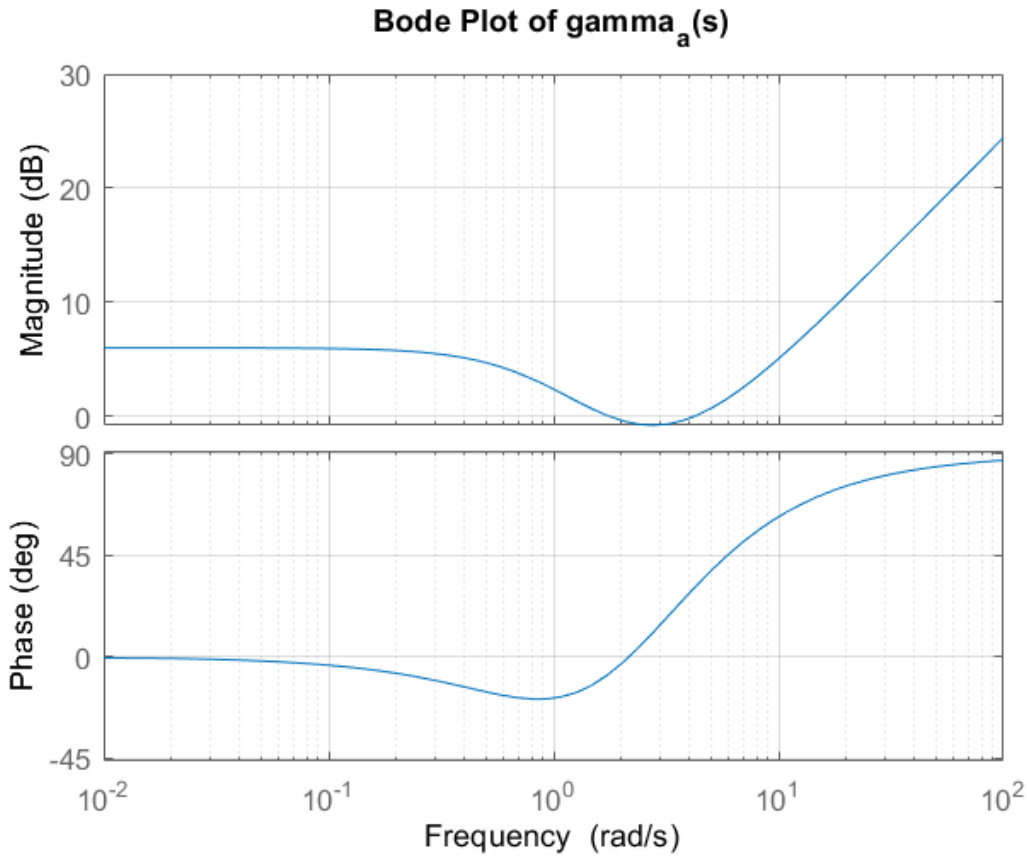

Fig. 5.5 Bode Plot of $\gamma_a(s)$

Figure 5.5 shows the Bode plot of $\gamma_a(s)$. The magnitude plot stays at approximately constant levels over the low-frequency range and starts to decrease until reaching the lowest level in the mid-frequency region.

Thereafter, its magnitude starts to increase rapidly and reaches relatively high levels at elevated frequencies which indicates that interaction effects become more important as the frequency increases.

The phase plot also remains almost unchanged at around zero until reaching the resonance region. In this region, it starts to move in a negative direction. Finally, it moves towards positive directions with increasing frequency up to about 90°.

The aforementioned characteristics of the Bode plot imply that the interaction of two output channels is highly frequency-dependent and increases significantly in the vicinity of the controller bandwidth region. The identified characteristics prove the existence of coupled dynamics due to the inductor used as well as the energy transfer process in the analyzed converter.

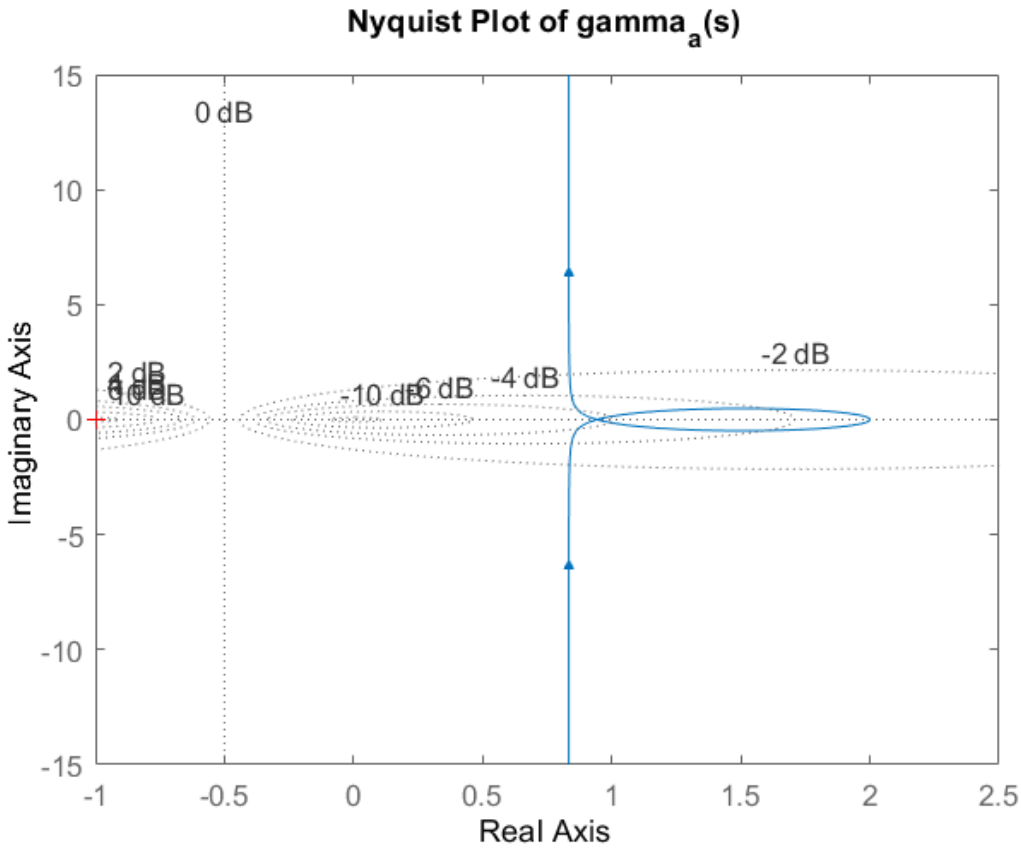

Fig. 5.6 Nyquist Plot of $\gamma_a(s)$

Figure 5.6 displays the Nyquist plot of $\gamma_a(s)$. The obtained response is located entirely in the right-half of the complex plane and does not exhibit any encirclement of the critical point (-1,0).

This fact implies that the interaction dynamics of the SIDO boost converter does not result in instability throughout the studied frequency range. The response maintains relatively safe distances from the critical point which shows that there are sufficient robustness margins for the closed-loop control system under consideration.

From the above, it can be concluded that the interaction dynamics do not adversely affect the stability of the closed-loop system. Therefore, properly-designed decentralized controllers can stabilize the studied converter in spite of the significant extent of coupling between its output channels.

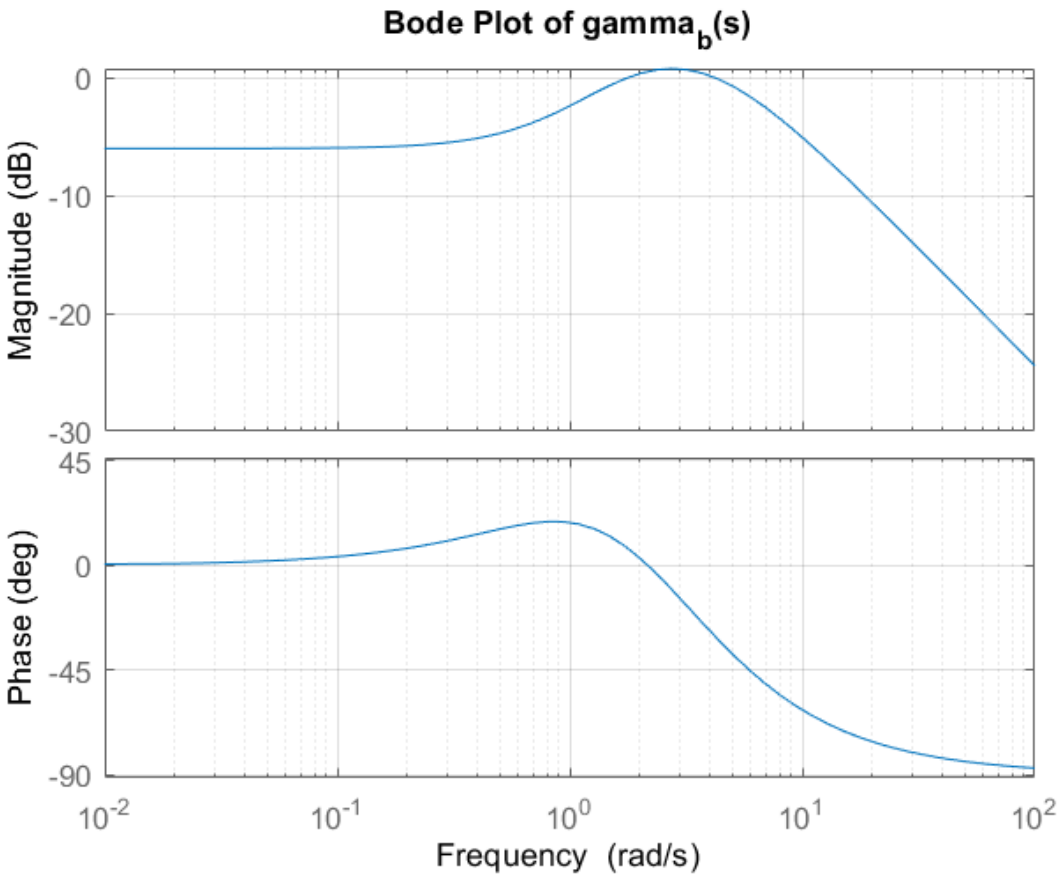

Fig. 5.7 Bode Plot of $\gamma_b(s)$

Figure 5.7 demonstrates the Bode plot of $\gamma_\beta(s)$. Unlike $\gamma_a(s)$, the magnitude plot exhibits a noticeable peak around the mid-frequency region which shows that the interaction is highly amplified. After the peak, its magnitude drops considerably with increasing frequency and stays at relatively low levels at elevated frequencies.

Meanwhile, the phase plot starts with small values of phases and then moves to positive regions with a steady increasing rate until reaching the value of -90°. Such a characteristic behavior of the phase plot implies the existence of directional coupling effect between the output channels of the analyzed converter.

The identified frequency-dependent interaction dynamics highlight the significance of determining proper controller bandwidths to minimize the extent of interaction.

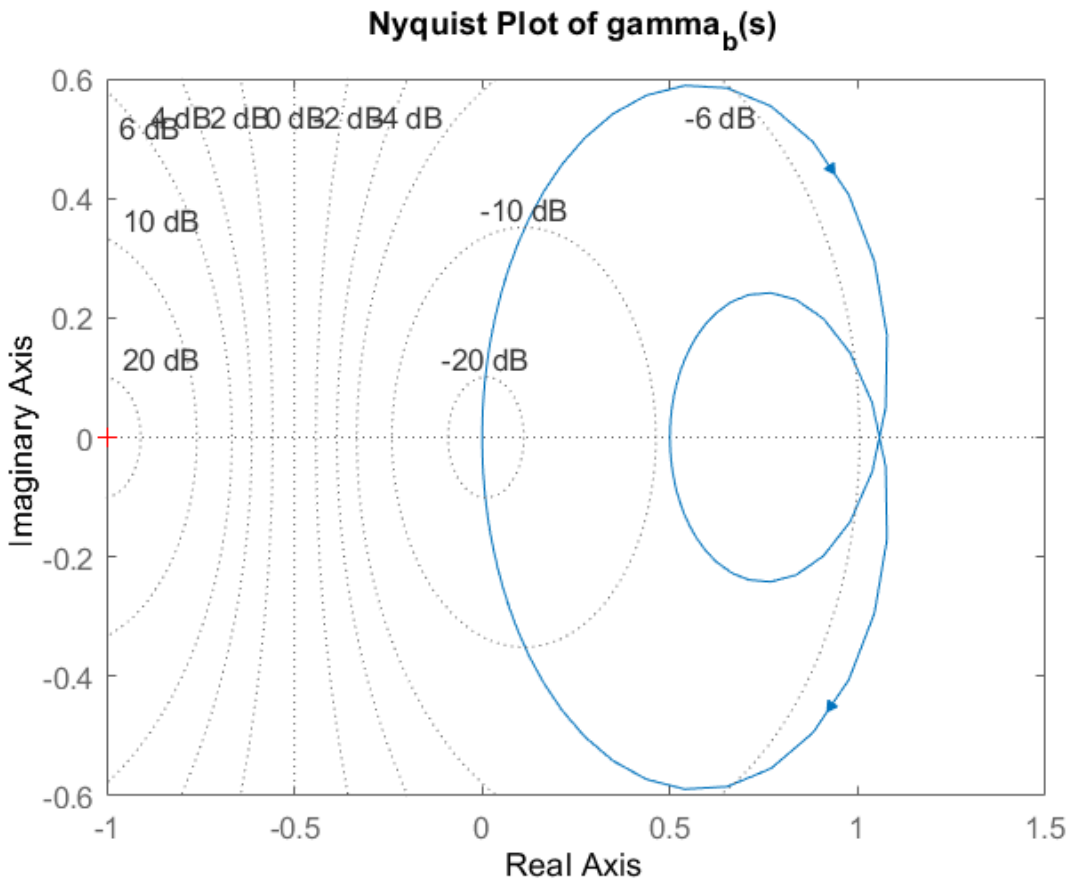

Fig. 5.8 Nyquist Plot of $\gamma_b(s)$

Figure 5.8 shows the Nyquist plot of $\gamma_\beta(s)$. As can be seen from the figure, the response does not exhibit any loop or encirclement of the critical point. Instead, it remains in the right-half plane of the complex frequency plane.

Such an observation indicates that the interaction dynamics are stable throughout the entire operational frequency range. The loop structure of the response is indicative of the characteristics obtained from the corresponding Bode response. In spite of the interaction amplification effect near the crossover-frequency region, there still exist sufficient robustness margins.

Thus, it can be concluded that the analyzed converter will be able to operate satisfactorily with the use of decentralized control strategy.

5.5 Decoupling and Stability Analysis

The effectiveness of the decentralized controller structure is investigated using decoupling analysis and loop transfer-function analysis.

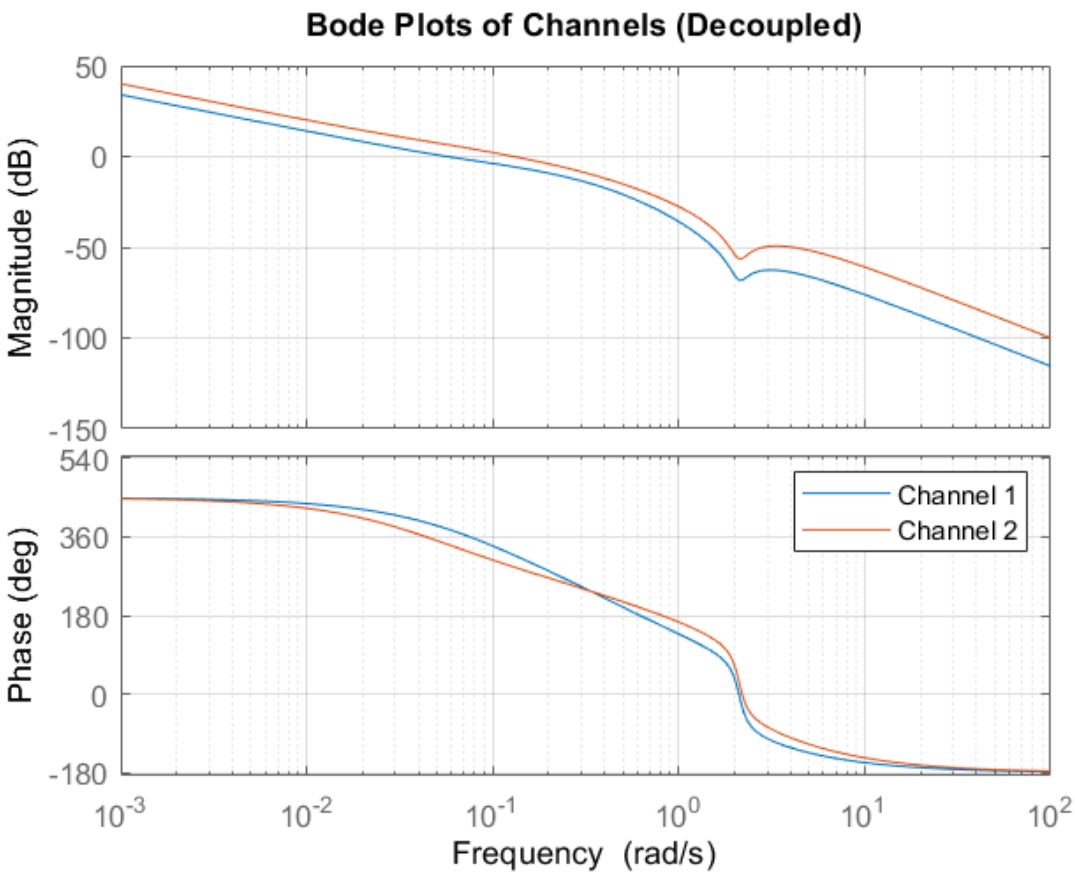

Fig. 5.9 Bode Plots of Channels

The Bode responses for the decoupled channels are shown in Figure 5.9 based on the proposed decentralized control structure design. From the responses, it can be noted that both channels have the same behavior of frequency responses with satisfactory behavior of the magnitude and phase responses across the entire frequency range. In addition, the magnitude responses have steady slopes of decreasing magnitudes with increasing frequencies and the phase responses have similar trends without fluctuations. The similarity in responses for Channel 1 and Channel 2 clearly shows that there was significant minimization of the interaction between output channels as a result of the effective operation of the decentralized controller in suppressing interaction amplification. Thus, satisfactory decoupling behavior was achieved through the use of the proposed control strategy.

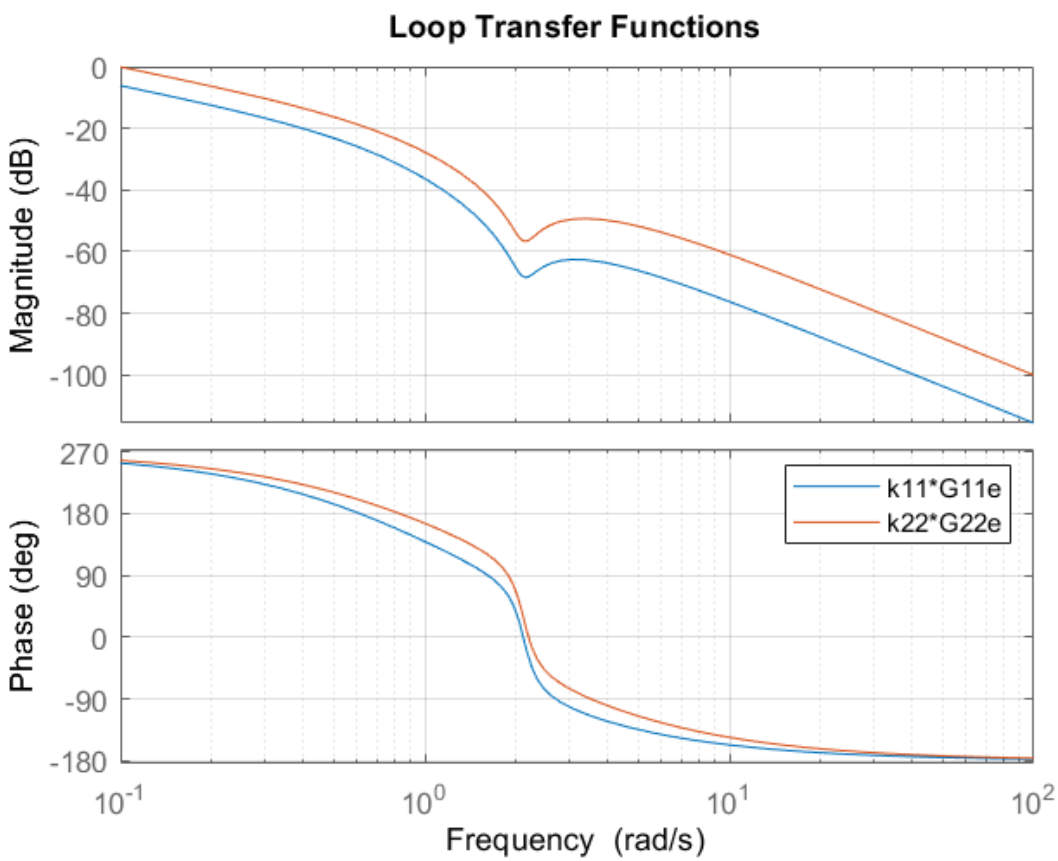

Fig. 5.10 Loop Transfer Functions

Figure 5.10 presents the responses of the loop transfer functions for the two control loops in the SIDO boost converter. It should be noted that the magnitude responses show crossover behavior with no excessive gain peaking at the crossover-frequency range. This means sufficient damping effects to avoid interaction resonance. On the other hand, the phase responses are gradually decreased with increasing frequencies. It is also evident from the figure that the two loop transfer functions have similar dynamic behaviors, leading to balanced closed-loop system performance. Therefore, sufficient stability and reduced interaction amplification are achieved as a result of the balanced crossover behavior.

The analyses facilitate the identification of interaction dominant frequency bands, robustness margins, crossover frequency behavior, damping characteristics, and stability of the system. Based on the results obtained, it is evident that the designed controller effectively alleviates interaction amplification, achieves channel independence, boosts robustness, and ensures stability of the converter operation

5.6 Closed-Loop Frequency Response Analysis

The closed-loop frequency responses are investigated for evaluating converter robustness and damping characteristics after controller implementation.

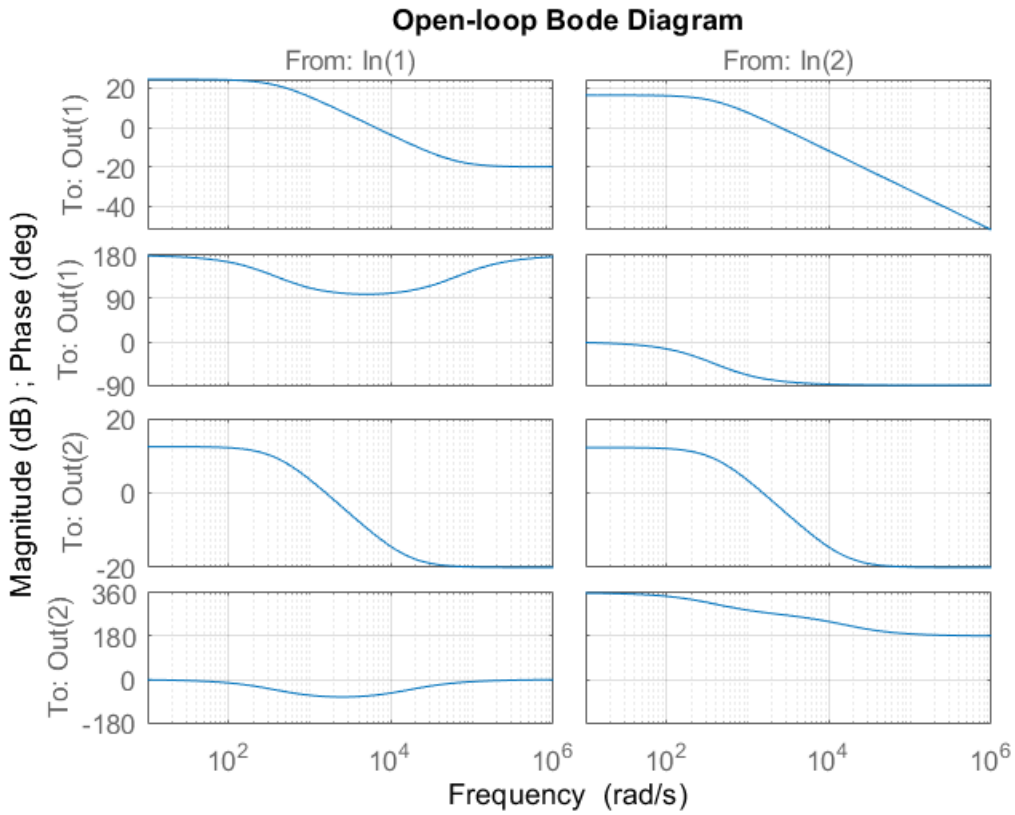

Fig. 5.11 Open-loop Bode Diagram

Figure 5.11 displays the open-loop Bode plot of the developed SIDO Boost Converter. Responses shown in this figure demonstrate the dynamic characteristics of the system output channels prior to applying the controller.

According to this plot, the magnitudes of both channels decrease when their frequency increases. At the same time, it should be noted that the phase plots differ significantly from one another.

The fact that the difference between the diagonal and off-diagonal responses exists confirms that there is some coupling between the output channels of the converter. All of the presented characteristics demonstrate the multivariable nature of the considered converter and the necessity to develop an interaction-aware controller.

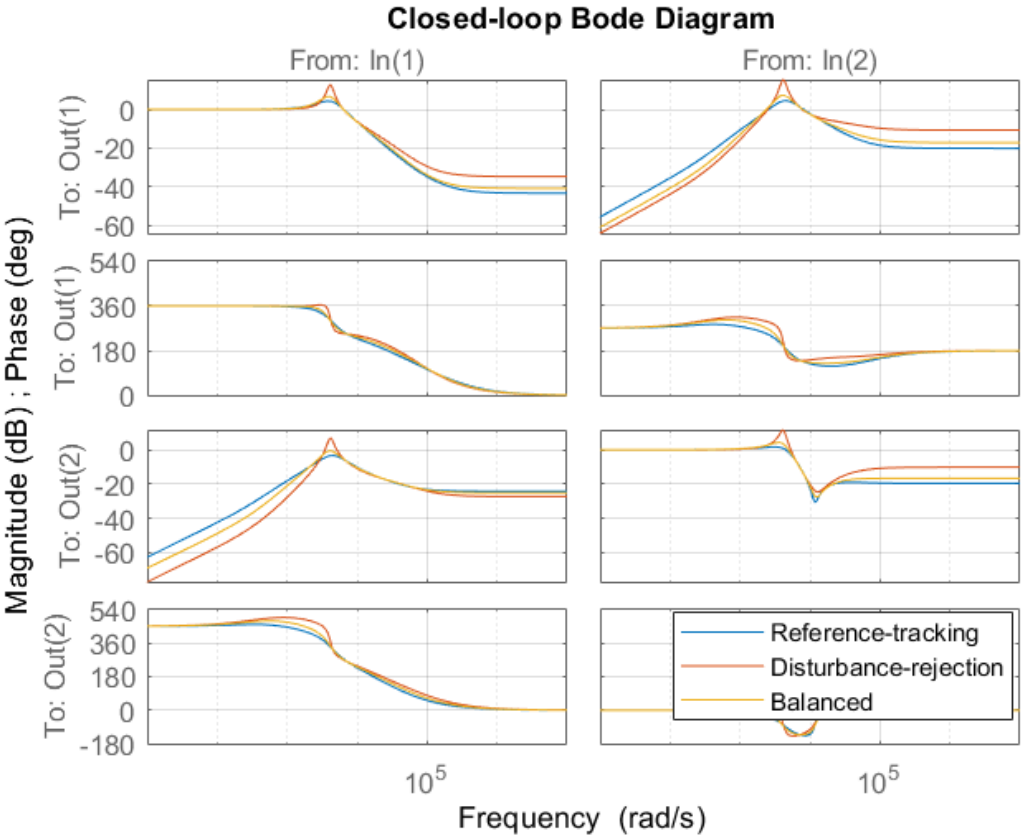

Fig. 5.12 MIMO Closed-loop Bode Diagram

Figure 5.12 displays the closed-loop Bode plots calculated via applying each of the three mentioned controller tuning techniques.

According to this figure, all controllers have improved frequency-domain properties of the converter, as well as allow establishing stable closed-loop operation. Moreover, it can be noticed that reference-tracking control produces the most responsive system and thus is characterized by high bandwidth properties.

Disturbance-rejection controller exhibits a better ability to attenuate low-frequency disturbances, whereas balanced controller tuning provides some compromise between these two methods

. Smoothness of closed-loop Bode responses implies that decentralized controller can successfully regulate two channels of the converter.

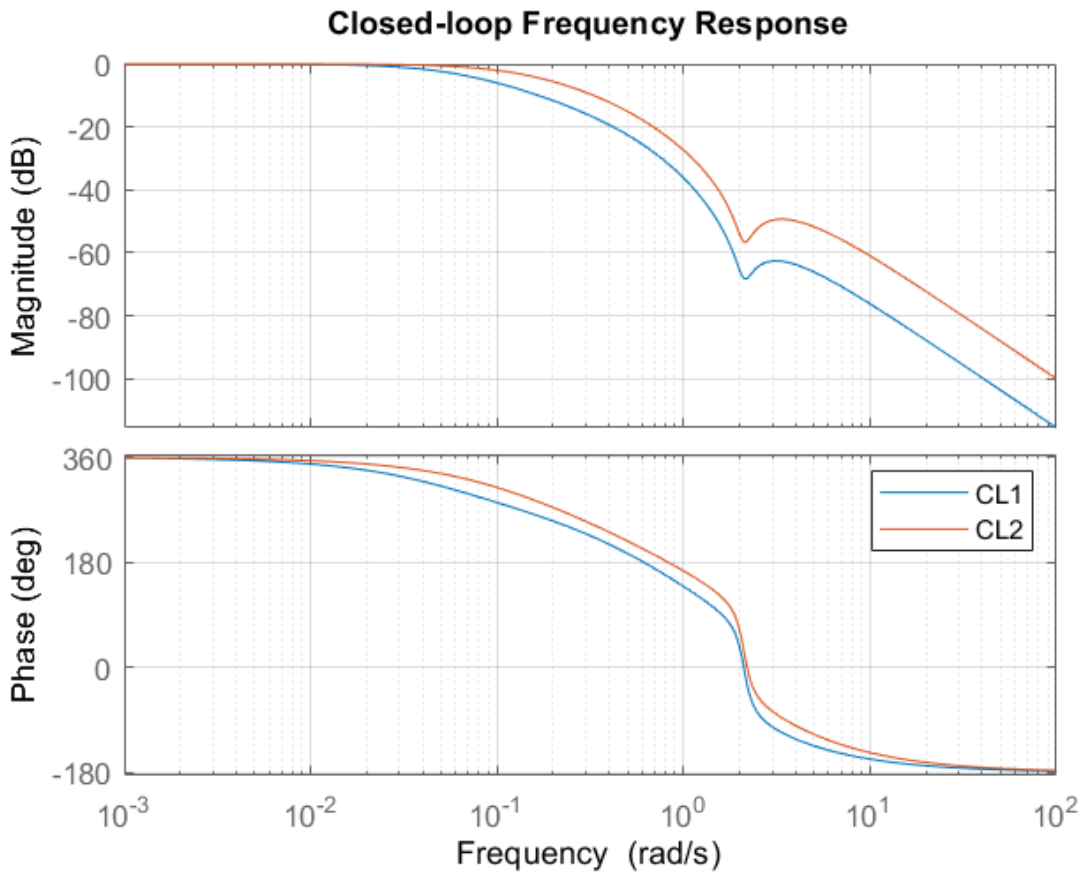

Fig. 5.13 Closed Loop Frequency response

Figure 5.13 demonstrates the frequency response of the developed SIDO converter. In addition, both of the closed-loop responses show the smooth character of magnitude and phase responses, along with acceptable crossover properties and damping characteristics. Magnitude response of the closed-loop responses remains close to unity in the low-frequency region, which confirms the capability of the converter to perform satisfactory tracking. Magnitudes begin to decline after the crossover frequency, while phase plots are also smooth and demonstrate no sharp transitions – it confirms the existence of sufficient stability margins in both cases.

5.7 Sensitivity Function Analysis

The sensitivity analysis is carried out for evaluating disturbance rejection capability and robustness characteristics.

The sensitivity function is represented as:

$$S(s) = (I + G(s)K(s))^{-1} \tag{5.3}$$

The complementary sensitivity function is represented as:

$$T(s) = I - S(s) \tag{5.4}$$

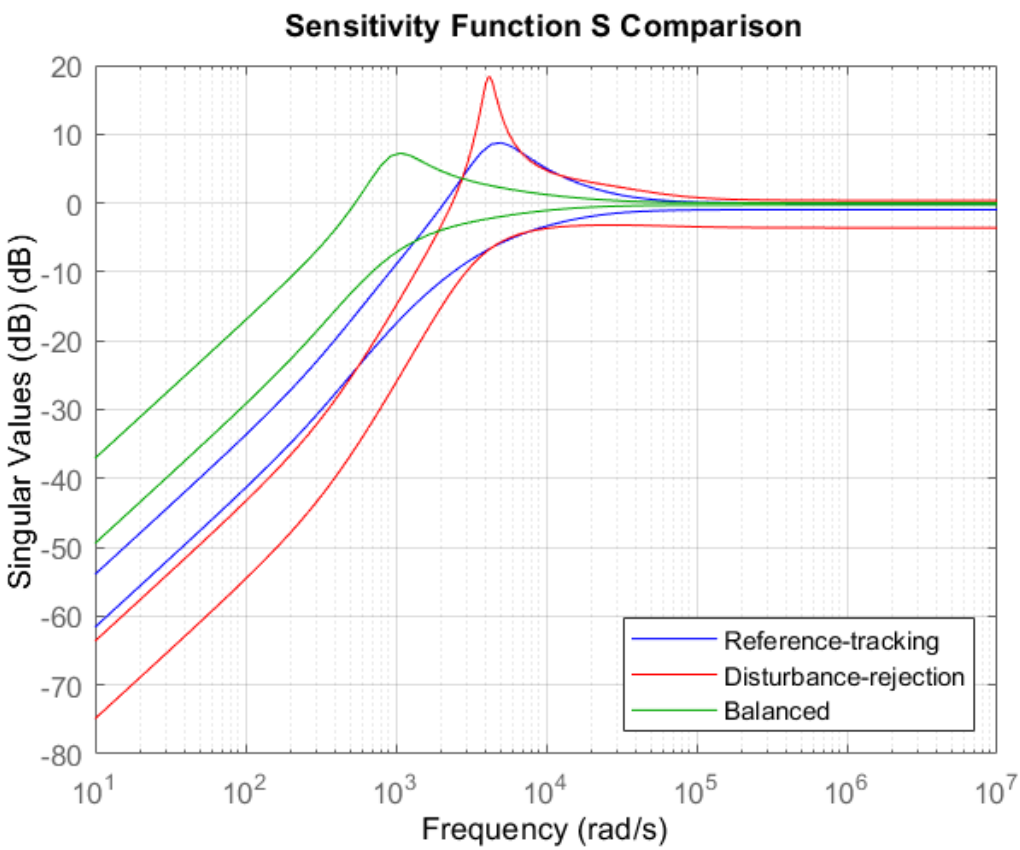

Fig. 5.14 Comparative Sensitivity Function S

Figure 5.14 presents comparison of the sensitivity functions calculated via each of the controller tuning techniques. Sensitivity function reflects the ability of the system to reject external disturbances as well as some features concerning robustness. Lower sensitivity of the system in the low-frequency region means that the ability of the converter to reject disturbances is higher. In this case, reference-tracking controller is characterized by high sensitivity because of its high bandwidth. On the other hand, disturbance-rejection controller allows achieving better robustness due to the low value of sensitivity.

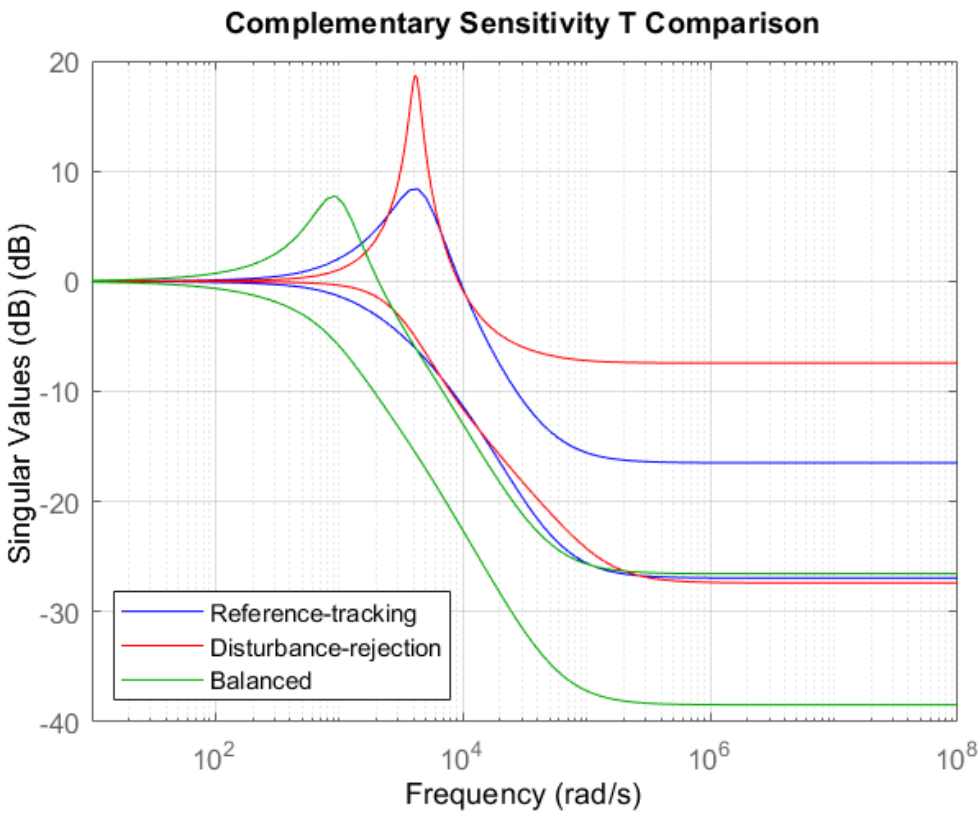

Fig. 5.15 Comparative Complementary Sensitivity Function *T*

Figure 5.5 shows the complementary sensitivity functions calculated through applying each of the three controller tuning methods. The main features revealed by this function include such aspects as sensitivity to measurement noise, bandwidth of the system, as well as amplification of resonances. In this case, reference-tracking controller shows a bigger peak in the crossover-frequency region. At the same time, disturbance-rejection controller possesses a more pronounced peak due to the emphasis on robustness properties. Finally, balanced controller demonstrates lower magnitude of the peak compared to reference-tracking one.

The balanced tuning therefore provides satisfactory robustness characteristics while maintaining acceptable transient performance.

5.8 Time-Domain Performance Analysis

The transient performance of the converter is investigated using comparative closed-loop step response analysis.

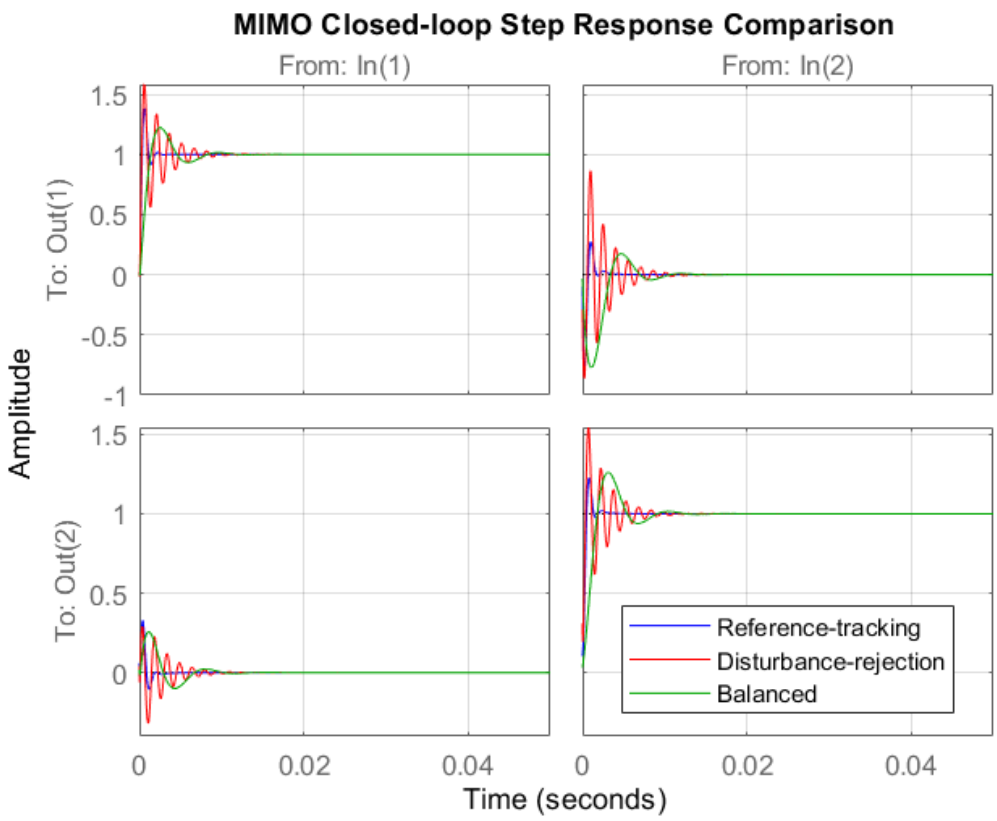

Fig. 5.16 Comparative MIMO Closed-loop Step Response

The obtained responses indicate that the reference-tracking controller provides faster transient response and reduced rise time. However, the aggressive tuning introduces increased oscillations and larger interaction sensitivity.

Figure 5.16 presents a comparison of the closed-loop responses obtained under applying each of the controller tuning techniques. As it can be seen, the step response obtained via applying reference-tracking controller tuning shows faster dynamics. However, there are relatively higher oscillations in this case.

Disturbance-rejection tuning method results in the slower step response with improved damping characteristics. Finally, balanced tuning produces a balance between the advantages of these two tuning techniques – the response is fast but has less oscillations. Thus, this solution is recommended due to the best combination of all the listed aspects.

5.9 Load Disturbance and Reference Tracking Analysis

The robustness characteristics of the converter are investigated under load disturbance and reference variation conditions.

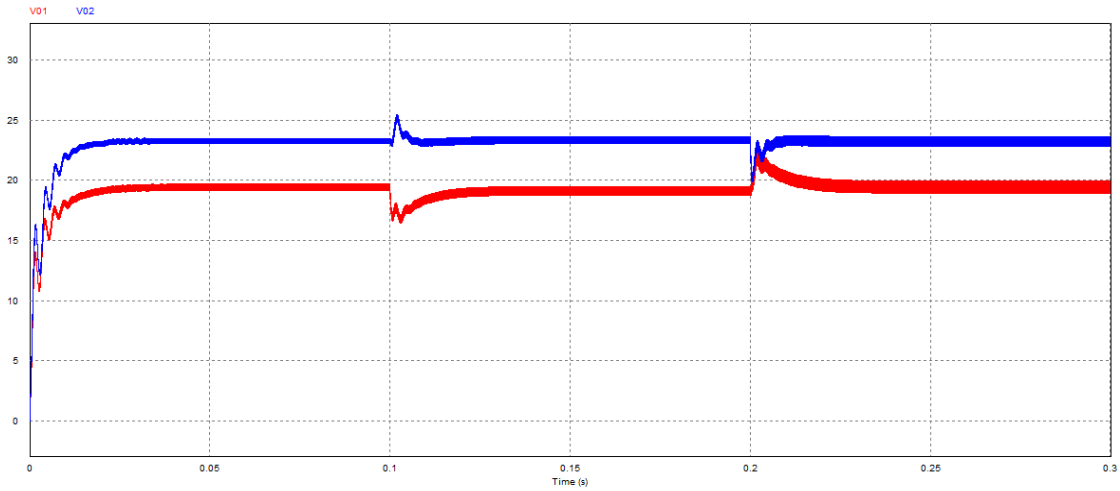

Fig. 5.17 Output Voltage Regulation under Load Variation

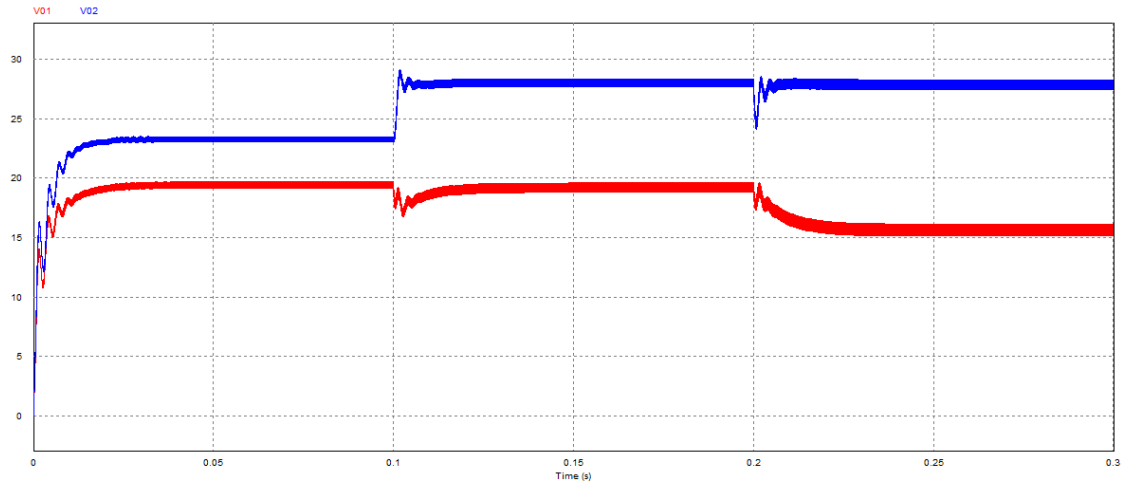

Fig. 5.18 Output Voltage Tracking under Reference Variation

The obtained responses indicate that the balanced controller effectively suppresses interaction-induced oscillations while maintaining satisfactory voltage regulation characteristics under varying operating conditions.

The disturbance responses confirm improved robustness and satisfactory transient recovery behaviour.

5.10 Comparative Controller Performance Analysis

TABLE 5.1 Comparative Controller Performance Analysis

Performance Parameter	Reference Tracking	Disturbance Rejection	Balanced Tuning
Rise Time	Fast	Moderate	Moderate
Settling Time	Low	Higher	Moderate
Overshoot	Higher	Low	Low
Disturbance Rejection	Moderate	Excellent	Good
Robustness	Moderate	High	High
Oscillations	Higher	Low	Low
Interaction Suppression	Moderate	Good	Excellent

From the comparative analysis, it is evident that reference-tracking tuning provides the fastest dynamic response, while disturbance-rejection tuning offers superior robustness against disturbances and parameter variations.

The balanced tuning approach combines the advantages of both methods and delivers the most effective overall performance. It achieves a satisfactory transient response together with improved damping characteristics, reduced interaction amplification between the output channels, and enhanced robustness margins.

As a result, the balanced controller provides a better compromise between speed, stability, and robustness, making it the most suitable controller configuration for the proposed Single-Inductor Dual-Output (SIDO) boost converter.

5.11 Discussion

The simulation results presented in this chapter validate the effectiveness of the developed mathematical model, interaction analysis methodology, and decentralized controller design for the proposed Single-Inductor Dual-Output (SIDO) boost converter. The obtained responses confirm the presence of strong interaction under open-loop conditions and demonstrate that the decentralized control structure significantly improves system stability and voltage regulation performance. Among the investigated tuning approaches, the balanced controller provides superior overall performance by effectively suppressing interaction amplification, improving damping characteristics, reducing cross-regulation effects, and maintaining satisfactory robustness under varying operating conditions. These results highlight the importance of interaction-aware controller tuning for achieving stable and reliable operation of multivariable DC–DC converter systems.

CHAPTER 6

CONCLUSION AND FUTURE SCOPE

6.1 Conclusion

The presented dissertation described modelling, interaction analysis, design of decentralized controllers, and simulation based-validation of a SIDO DC-DC boost converter system. Due to the presence of a single inductor, the converter displays significant dynamic interactions between its two output ports and is considered as an MIMO system. An accurate small-signal model of the converter has been formulated, representing it in the form of a transfer function matrix. As seen from the derived transfer function matrix, there were non-zero off-diagonal transfer functions showing the presence of significant interactions between the output ports in the form of cross-regulation. Relative Gain Array (RGA), Hankel Interaction Index Array (HIIA), interaction index analysis with respect to the H2-norm, singular value decomposition analysis, gamma functions, Bode plot analysis, and Nyquist diagram analysis have been used to study the interaction properties of the converter system. As concluded from the obtained results, there is significant dynamic coupling, interaction amplification near crossover frequencies, reduced loop independence, and frequency dependency of interactions.

Taking into account the results of the interaction analysis, decentralized PIDF controllers have been designed using the reference-tracking, disturbance-rejection, and balanced tuning methods. The reference-tracking controller ensures faster dynamics and higher bandwidth, but increases interaction sensitivity. The disturbance-rejection controller provides better damping and robustness at the cost of poor dynamic performance. The balanced controller achieves a good trade-off between reference tracking, disturbance rejection, robustness, and interaction suppression. Extensive simulation results in MATLAB/Simulink environment under both open-loop and closed-loop operations have shown that the balanced controller is effective in terms of providing smoother transient response, adequate damping and robustness characteristics, reduced cross-regulation effects, and voltage regulation. Thus, the proposed decentralized control scheme

considering interactions can be successfully used in the case of multi-output DC-DC converter systems.

6.2 Future Scope

While the current study successfully addressed the problem of interaction analysis and design of decentralized controllers for SIDO DC-DC converter, several important areas require future research. More advanced multivariable control schemes such as Model Predictive Control (MPC), Sliding Mode Control (SMC), Adaptive Control, and Robust H∞ Control can be considered. Artificial intelligence (AI)-based controller tuning schemes such as Fuzzy Logic Control, Neural Network Control, and Reinforcement Learning-based control could also be studied.

The current work can also be generalized to other multi-output DC-DC converters and other applications such as power conversion systems involving renewables, power converters for electric vehicles, and DC microgrids. Analysis of interaction effects under uncertain parameter variations, switching nonlinearities, sensing noise, and aging can be included in future work. Furthermore, Hardware-in-the-Loop (HIL) implementation of the proposed interaction-aware decentralized controller, and experimental validation using prototypical circuits can be performed in the future. Optimization-based tuning of the controllers for fast dynamic response, robustness enhancement, and reduction in interaction could be performed in the future.

LIST OF PUBLICATIONS

Table X: List of Publications

Publisher	Name of Paper	Scopus Indexed	Status
COMPENG 2026 (Castel Ivano, ITALY)	Individual Channel based control framework for Single-Inductor Double-Output DC-DC Boost Converter Systems	YES	Accepted
Springer PICS 2026 (NIT Hamirpur)	Decentralized Control of a Single-Inductor Dual-Output Boost Converter for Improved Tracking and Disturbance Suppression	YES	Accepted
Springer PICS 2026 (NIT Hamirpur)	Analysis of frequency dependent tools for interaction quantification of Single-inductor Double-output (SIDO) DC-DC Boost Converter System	YES	Accepted

APPENDICES

APPENDIX 1: CONFERENCES

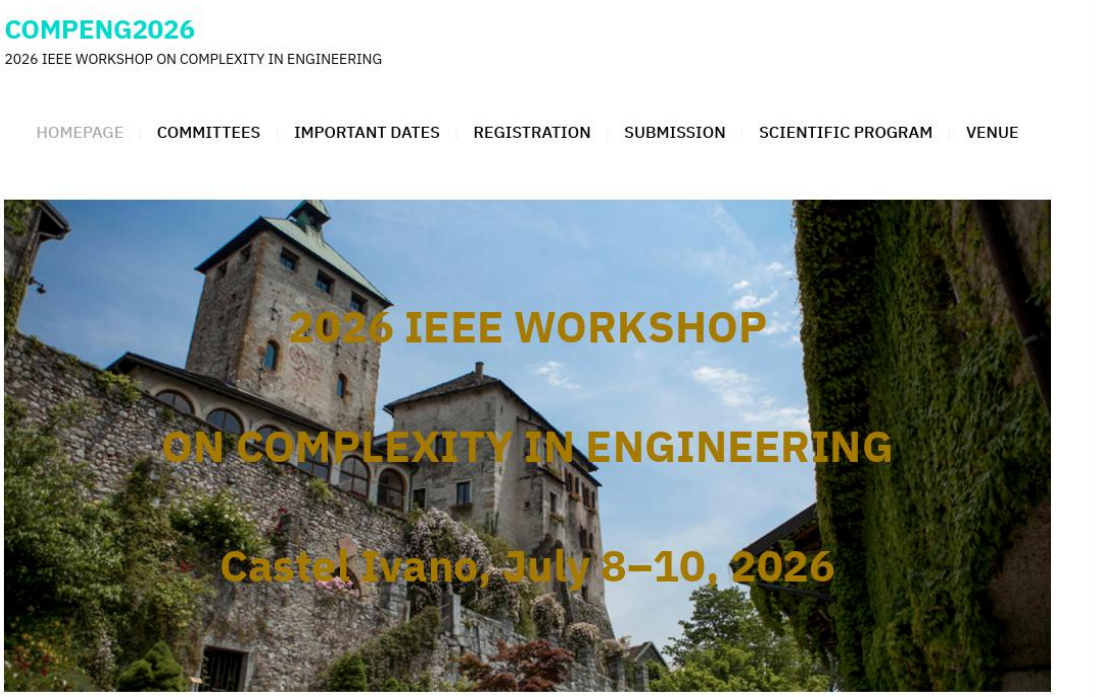

Figure A.1: COMPENG 2026

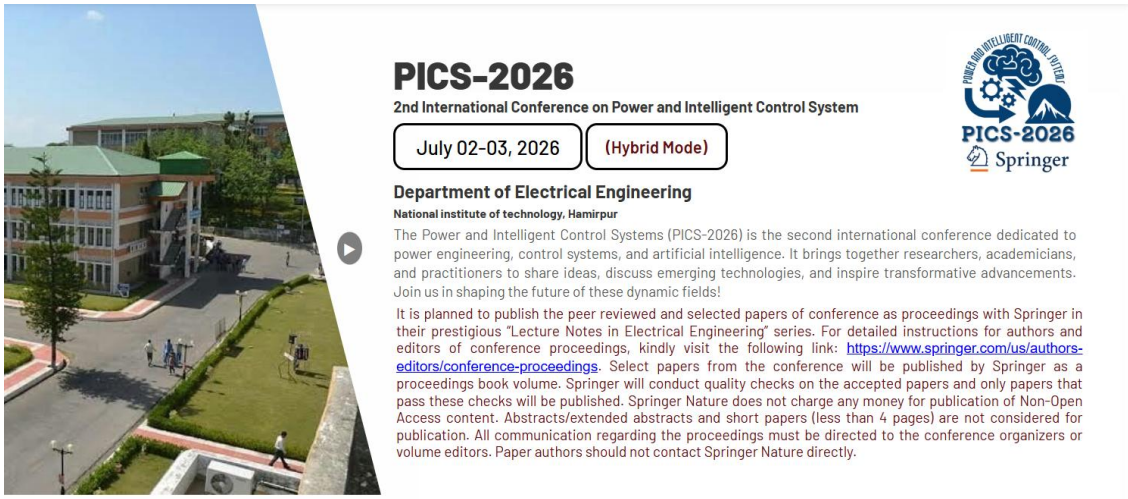

Figure A.2: Springer PICS 2026

APPENDIX 2: PAPER ACCEPTANCE PROOF

Gmail Daksh Jangra <dakshdtu@gmail.com>

Fwd: COMPENG 2026 – Abstract Acceptance (Oral Contribution)

To: dakshdtu@gmail.com <dakshdtu@gmail.com> Tue, 19 May at 5:36 PM

From: <compeng.2026@ino.cnr.it>
Date: Sun, 10 May 2026, 10:40 pm
Subject: COMPENG 2026 – Abstract Acceptance (Oral Contribution)
To:

Dear Author,

We are pleased to inform you that your abstract has been accepted for an **oral presentation** at COMPENG 2026.

Each talk will be up to **20 minutes**, followed by **5 minutes** for questions.

We will notify you as soon as the conference program becomes available. In the meantime, if you have any specific scheduling requests, please let us know by **May 20**.

If you require a visa invitation letter, please send an email to compeng.2026@ino.cnr.it including a scanned copy of your passport.

Please note that presenting at the conference requires prior registration. **The early registration deadline is May 31.**

We also recommend **booking your accommodation in Levico Terme** as soon as possible. Instructions are available on the conference website:

https://compeng2026.ino.cnr.it/venue/

We look forward to welcoming you to COMPENG 2026.

Best regards,
The COMPENG 2026 Organizing Committee

Figure A.3: Acceptance Mail for COMPENG 2026

Gmail 24/C&I/08 DAKSH <daksh_24ci08@dtu.ac.in>

Notification of Submission in PICS-2026 Conference (Paper ID: #148)

Microsoft CMT <noreply@msr-cmt.org> Sun, 31 May at 6:13 PM
To: DAKSH . <daksh_24ci08@dtu.ac.in>

Dear Authors,
We are pleased to inform you that your paper titled "Analysis of frequency dependent tools for interaction quantification of Single-inductor Double-output (SIDO) DC-DC Boost Converter System " (Submission ID: #148), has been provisionally accepted for presentation at the PICS-2026 conference, scheduled to take place from July 2-3, 2026, at NIT Hamirpur, (H.P.), India, in hybrid mode.

Kindly submit the Camera-Ready Paper by 5 June 2026, after addressing all the reviewer comments by logging in to your CMT account.

Important Notes:
[1] The Camera-Ready Paper must be strictly in the Springer Conference Paper Format (figures captions, tables, headings, references, etc.). Ensure margins are strictly as per template. The templates are available in the following links:

MS Word:
https://drive.google.com/file/d/1tYPp2cGK2BS4f4fB8EqpTLRvzEqIXaxz/view

Latex:
https://www.overleaf.com/latex/templates/springer-conference-proceedings-template-updated-2022-01-12/wcvbtmwtykqj

[2] Proofread your manuscript thoroughly to confirm that it will require no revision. Ensure all references are valid and appear in increasing order in the manuscript. Detection of any invalid reference can lead to rejection of paper at any stage.

[3] The acceptance is subject to the final plagiarism, AI percentage, quality check and satisfactory incorporation of reviewer comments (available on the Microsoft CMT Portal) and the submission will be checked for a Similarity score and AI percentage below 20%, as determined by plagiarism and AI detection tools.

[4] Prepare a response sheet detailing how each of the reviewers' comments have been addressed. Create a file named after your Submission ID (e.g. 123_response.pdf) containing the compliance report to reviewers' comments.

[5] Kindly upload the camera-ready paper (e.g. 123.pdf for the camera-ready file name) and supplementary file (123_response.pdf) in CMT by 5 June 2026. For CMT upload, please use ONLY the PDF format. However, in the registration Google form, uploading the Word (or) Latex zip file of the camera-ready paper will also be required.

[6] Please note that the paper will be considered "Accepted" only after completion of both the Registration Google form and submission of the Camera-Ready Paper.

[7] The registration procedure is available in the following link: https://pics2026nith.com/Registration. We have added an option of hybrid mode of presentation (offline/in-person) in the registration Google form.

In case of any query, kindly reach out to any of the Conference Organizing Committee members.

Regards,
PICS-2026 Organizing Committee
https://pics2026nith.com

Please do not reply to this email as it was generated from an email account that is not monitored.

To stop receiving conference emails, you can check the 'Do not send me conference email' box from your User Profile.

Microsoft respects your privacy. To learn more, please read our Privacy Statement.

Microsoft Corporation
One Microsoft Way
Redmond, WA 98052

Figure A.4: Acceptance Mail for PICS 2026 1st paper

Gmail 24/C&I/08 DAKSH <daksh_24ci08@dtu.ac.in>

Notification of Submission in PICS-2026 Conference (Paper ID: #554)

Microsoft CMT <noreply@msr-cmt.org> Sun, 31 May at 6:13 PM
To: DAKSH . <daksh_24ci08@dtu.ac.in>

Dear Authors,
We are pleased to inform you that your paper titled "Decentralized Control of a Single-Inductor Dual-Output Boost Converter for Improved Tracking and Disturbance Suppression" (Submission ID: #554), has been provisionally accepted for presentation at the PICS-2026 conference, scheduled to take place from July 2-3, 2026, at NIT Hamirpur, (H.P.), India, in hybrid mode.

Kindly submit the Camera-Ready Paper by 5 June 2026, after addressing all the reviewer comments by logging in to your CMT account.

Important Notes:
[1] The Camera-Ready Paper must be strictly in the Springer Conference Paper Format (figures captions, tables, headings, references, etc.). Ensure margins are strictly as per template. The templates are available in the following links:

MS Word:
https://drive.google.com/file/d/1tYPp2cGK2BS4f4fB8EqpTLRvzEqIXaxz/view

Latex:
https://www.overleaf.com/latex/templates/springer-conference-proceedings-template-updated-2022-01-12/wcvbtmwtykqj

[2] Proofread your manuscript thoroughly to confirm that it will require no revision. Ensure all references are valid and appear in increasing order in the manuscript. Detection of any invalid reference can lead to rejection of paper at any stage.

[3] The acceptance is subject to the final plagiarism, AI percentage, quality check and satisfactory incorporation of reviewer comments (available on the Microsoft CMT Portal) and the submission will be checked for a Similarity score and AI percentage below 20%, as determined by plagiarism and AI detection tools.

[4] Prepare a response sheet detailing how each of the reviewers' comments have been addressed. Create a file named after your Submission ID (e.g. 123_response.pdf) containing the compliance report to reviewers' comments.

[5] Kindly upload the camera-ready paper (e.g. 123.pdf for the camera-ready file name) and supplementary file (123_response.pdf) in CMT by 5 June 2026. For CMT upload, please use ONLY the PDF format. However, in the registration Google form, uploading the Word (or) Latex zip file of the camera-ready paper will also be required.

[6] Please note that the paper will be considered "Accepted" only after completion of both the Registration Google form and submission of the Camera-Ready Paper.

[7] The registration procedure is available in the following link: https://pics2026nith.com/Registration. We have added an option of hybrid mode of presentation (offline/in-person) in the registration Google form.

In case of any query, kindly reach out to any of the Conference Organizing Committee members.

Regards,
PICS-2026 Organizing Committee
https://pics2026nith.com

Please do not reply to this email as it was generated from an email account that is not monitored.

To stop receiving conference emails, you can check the 'Do not send me conference email' box from your User Profile.

Microsoft respects your privacy. To learn more, please read our Privacy Statement.

Microsoft Corporation
One Microsoft Way
Redmond, WA 98052

Figure A.5: Acceptance Mail for PICS 2026 2nd paper

REFERENCES

[1] E. H. Bristol, "On a New Measure of Interaction for Multivariable Process Control," *IEEE Trans. Autom. Control*, vol. 11, no. 1, pp. 133–134, 1966, doi:10.1109/TAC.1966.1098266.

[2] S. Skogestad and I. Postlethwaite, *Multivariable Feedback Control: Analysis and Design*, 2nd ed. Chichester, U.K.: Wiley, 2005, doi:10.1002/9781119174298.

[3] B. Wittenmark and M. E. Salgado, "Hankel-norm Based Interaction Measure for Input–Output Pairing of Multivariable Systems," in *Proc. 43rd IEEE Conf. Decision and Control*, 2004, pp. 810–815, doi:10.1109/CDC.2004.1428609.

[4] M. E. Salgado and A. C. Conley, "MIMO Interaction Measure and Controller Structure Selection," *Int. J. Adapt. Control Signal Process.*, vol. 17, no. 1–2, pp. 59–75, 2003, doi:10.1002/acs.678.

[5] A. C. Conley and M. E. Salgado, "Gramian Based Interaction Measure," in *Proc. IFAC Workshop Adaptive Systems in Control and Signal Processing*, 2001, doi:10.1016/S1474-6670(17)48919-7.

[6] M. R. Moaveni and W. Birk, "Modified Hankel Interaction Index Array for Input–Output Pairing," *J. Process Control*, vol. 18, no. 7–8, pp. 641–652, 2008, doi:10.1016/j.jprocont.2007.12.006.

[7] P. Thota, A. R. B. Chivukula, and V. V. S. B. R. Chintapalli, "Selection of Input–Output Pairing for Multi-Input Multi-Output Systems," *ISA Trans.*, vol. 52, no. 5, pp. 596–604, 2013, doi:10.1016/j.isatra.2013.04.009.

[8] M. Manogna, B. A. Reddy, and K. Padma, "Interaction Measures in a Three-Input Integrated DC–DC Converter," *IET Power Electron.*, vol. 15, no. 3, pp. 356–365, 2022, doi:10.1049/pel2.12125.

[9] J. D. Dasika, B. Bahrani, M. Saeedifard, A. Karimi, and A. Rufer, "Multivariable Control of Single-Inductor Dual-Output Boost Converter," *IEEE Trans. Ind. Appl.*, vol. 50, no. 1, pp. 259–269, 2014, doi:10.1109/TIA.2013.2266616.

[10] B. Bahrani, J. D. Dasika, M. Saeedifard, A. Karimi, and A. Rufer, "Multivariable Control of Single-Inductor Dual-Output Boost Converters," *IEEE Trans. Power Electron.*, vol. 29, no. 3, pp. 1179–1188, 2014, doi:10.1109/TPEL.2013.2266616.

[11] S. A. Augusti Lindiya, N. Subashini, and K. Vijayarekha, "Cross Regulation Reduced Optimal Multivariable Controller Design for a Multi-Output Boost Converter," *Int. J. Power Electron. Drive Syst.*, vol. 11, no. 1, pp. 47–56, 2020, doi:10.11591/ijpeds.v11.i1.pp47-56.

[12] L. Indiiya, N. Subashini, and K. Vijayarekha, "Design and Control of a Bipolar-Output MIMO DC–DC Converter," *Energies*, vol. 14, no. 11, p. 3122, 2021, doi:10.3390/en14113122.

[13] P. Thota, A. R. B. Chivukula, and V. V. S. B. R. Chintapalli, "Participation Factor-Based Analysis of Cross-Regulation in Dual-Output DC Converters," *Eng. Sci. Technol. Int. J.*, vol. 21, no. 2, pp. 329–337, 2018, doi:10.1016/j.jestch.2017.12.002.

[14] H. Zhang, M. Jing, W. Liu, and F. Deng, "Design-Oriented Analysis of Cross-Regulation in Single-Inductor Dual-Output Buck–Boost Converters," *Int. J. Circuit Theory Appl.*, vol. 49, no. 12, pp. 3966–3993, 2021, doi:10.1002/cta.3083.

[15] L. Yang, Y. Pan, and X. Deng, "Robust Control for Non-Minimum Phase and Cross-Regulation in Single-Inductor Dual-Output Converters," *Eng. Appl. Artif. Intell.*, vol. 120, p. 105611, 2023, doi:10.1016/j.engappai.2023.105611.

[16] K. J. Åström and T. Hägglund, *Advanced PID Control*. Research Triangle Park, NC, USA: ISA, 2006, doi:10.5555/1121746.

[17] S. Skogestad, "Control Structure Design for Complete Chemical Plants," *Comput. Chem. Eng.*, vol. 25, no. 2–3, pp. 219–234, 2001, doi:10.1016/S0098-1354(00)00450-8.

[18] J. M. Maciejowski, *Multivariable Feedback Design*. Reading, MA, USA: Addison-Wesley, 1989, doi:10.1109/9780470545105.

[19] H. P. Huang and J. C. Jeng, "Automatic Tuning of Decentralized PID Controllers Based on Relative Gain Array," *IEEE Trans. Ind. Electron.*, vol. 64, no. 5, pp. 4007–4017, 2017, doi:10.1109/TIE.2016.2641058.

[20] S. Zhou, G. Zhou, G. Liu, and G. Mao, "Small-Signal Modeling and Cross-Regulation Suppression for a Current-Mode Controlled SIDO Buck Converter," *IET Power Electron.*, vol. 11, no. 14, pp. 2308–2317, 2018, doi:10.1049/iet-pel.2018.5727.

[21] X. Liu, J. Xu, J. Wang, and Q. Mu, "A Single-Inductor Dual-Output Buck Converter with Pulse-Train Control," in *Proc. IEEE Int. Symp. Power Electron. Distributed Generation Systems*, 2010, pp. 449–452.

[22] W. Xu, Y. Li, X. Gong, and Z. Hong, "A Single-Inductor Dual-Output Converter with Low Ripples and Improved Cross-Regulation," in *Proc. IEEE Custom Integrated Circuits Conf.*, 2009, pp. 303–306.

[23] W. Xu, Y. Li, X. Gong, and Z. Hong, "A Dual-Mode Single-Inductor Dual-Output Switching Converter with Small Ripple," *IEEE Trans. Power Electron.*, vol. 25, no. 3, pp. 614–623, 2010, doi:10.1109/TPEL.2009.2033927.

[24] D. Trevisan, P. Mattavelli, and P. Tenti, "Digital Control of Single-Inductor Multiple-Output DC–DC Converters in CCM," *IEEE Trans. Ind. Electron.*, vol. 55, no. 9, pp. 3476–3483, 2008, doi:10.1109/TIE.2008.927505.

[25] M. H. Huang, K. H. Chen, and W. H. Wei, "Single-Inductor Dual-Output DC–DC Converter Control with Improved Efficiency," in *Proc. IEEE MWSCAS*, 2007, pp. 550–553.

[26] W. H. Chang, J. H. Wang, and C. H. Tsai, "A Peak-Current Controlled SIDO DC–DC Buck Converter with Time-Multiplexing," in *Proc. IEEE VLSI-DAT*, 2010, pp. 331–334.

[27] J. Ding, Y. Zhang, and Z. Sun, "Digital Twin-Based Control for Cross-Regulation Compensation in SIDO Converters," *Int. J. Electr. Power Energy Syst.*, vol. 101, pp. 394–404, 2018, doi:10.1016/j.ijepes.2018.05.084.

[28] S. Zitzler, M. Kuzlu, and M. Karimi, "LQR Control with Cross-Coupling Compensation for Single-Inductor Multi-Output Converters," in *Proc. IET PEMD*, 2014, doi:10.1049/cp.2014.0558.

[29] L. Wang, J. Xu, and Y. Zhao, "Feedforward Decoupling Control of Dual-Output DC–DC Converter," in *Proc. IEEE ECCE*, 2016, pp. 1–6, doi:10.1109/ECCE.2016.7741743.

[30] M. Xie, X. Shen, and D. Xu, "Simplified Control of Multiple-Output Buck Converters Based on Sliding-Mode Techniques," *Electr. Power Components Syst.*, vol. 43, no. 4, pp. 379–388, 2015, doi:10.1080/15325008.2014.994547.

[31] J. Guo and F. Zare, "Optimal Power Flow with Multi-Output DC–DC Converter Loads," *IEEE Trans. Power Syst.*, vol. 27, no. 1, pp. 370–378, 2012, doi:10.1109/TPWRS.2011.2169398.

[32] P. Thota, V. V. S. Chintapalli, A. R. B. Chivukula, and K. J. Kumar, "Participation Factor-Based Output Feedback Controller Design for MIMO Systems," *IEEE Trans. Control Syst. Technol.*, vol. 18, no. 1, pp. 212–219, 2010, doi:10.1109/TCST.2009.2025629.

[33] T. Sato, T. Tazawa, and H. Akagi, "Voltage-Control Strategy for Dual-Output Boost Converters," *IEEE Trans. Ind. Appl.*, vol. 49, no. 2, pp. 710–718, 2013, doi:10.1109/TIA.2012.2234734.

[34] C. Gou, X. Du, and B. Zhang, "Cross-Coupling Decoupling Control for Multi-Output Converters," in *Proc. IEEE APEC*, 2018, pp. 1340–1344, doi:10.1109/APEC.2018.8341050.

[35] M. Nakano and S. Murao, "Observer-Based Control to Suppress Cross-Regulation in Dual-Output Converters," *IEEE Trans. Power Electron.*, vol. 34, no. 6, pp. 5916–5924, 2019, doi:10.1109/TPEL.2018.2873721.

[36] K. Aggarwal and S. Mitra, "Analysis of Power Imbalance in Cascaded SIMO Converters," *Renew. Energy*, vol. 132, pp. 1265–1273, 2019, doi:10.1016/j.renene.2018.09.068.

[37] R. Bajpai, A. Yadav, and A. Kulkarni, "Decentralized Control of Modular Multi-Output Converters," *IEEE Trans. Ind. Electron.*, vol. 69, no. 7, pp. 6364–6373, 2022, doi:10.1109/TIE.2021.3120592.

[38] Y. Sun, X. Wu, and M. Zhao, "Single-Inductor Dual-Output Converter with Dynamic Power Distribution," in *Proc. IEEE ASIC Conf.*, 2009, pp. 1097–1100.

[39] C. Y. Tsui and W. H. Ki, "Single-Inductor Multiple-Output Converters with Time-Multiplexing Control," *IEEE J. Solid-State Circuits*, vol. 38, no. 1, pp. 89–100, 2003, doi:10.1109/JSSC.2002.806040.

[40] D. Ma, W. H. Ki, and C. Y. Tsui, "A Pseudo-CCM/DCM SIMO Converter with Freewheel Switching," *IEEE J. Solid-State Circuits*, vol. 38, no. 6, pp. 1007–1014, 2003, doi:10.1109/JSSC.2003.820117.

[41] H. P. Le, C. S. Chae, K. C. Lee, S. W. Wang, and G. H. Cho, "A Single-Inductor DC–DC Converter with Five Outputs and Ordered Power-Distributive Control," *IEEE J. Solid-State Circuits*, vol. 42, no. 12, pp. 2706–2714, 2007, doi:10.1109/JSSC.2007.909279.

[42] J. M. Zinck and A. Stankovic, "Modeling and Simulation of Multi-Output DC–DC Converters in Power Systems," *IEEE Trans. Power Syst.*, vol. 23, no. 4, pp. 1913–1920, 2008, doi:10.1109/TPWRS.2008.2001420.

[43] T. Rupf, L. Reindl, and B. Bettermann, "Fundamentals of Single-Inductor Dual-Output Converters for Micro-Power Systems," *IEEE Trans. Ind. Electron.*, vol. 58, no. 8, pp. 3347–3359, 2011, doi:10.1109/TIE.2010.2108262.

[44] J. H. Yoon and Y. K. Kim, "Fractional-Order Control of Single-Inductor Dual-Output Converters," *IEEE Trans. Power Electron.*, vol. 34, no. 12, pp. 11872–11884, 2019, doi:10.1109/TPEL.2019.2902588.

[45] Y. Tsuruta, S. Yokoyama, H. Nishimura, and T. Higuchi, "Multi-Loop Control of SIDO Boost Converter for Photovoltaics," *Renew. Energy*, vol. 80, pp. 584–594, 2015, doi:10.1016/j.renene.2014.12.047.

[46] M. Mirzanejad and H. Moayedi, "Output-Regulation in Dual-Output Converters Using H∞ Control," *IEEE Trans. Ind. Appl.*, vol. 55, no. 6, pp. 7264–7272, 2019, doi:10.1109/TIA.2019.2935341.

[47] T. Ivanov and D. Bakker, "Design Method for Output Prioritization in Single-Inductor Converters," *Energy Convers. Manage.*, vol. 149, pp. 780–789, 2017, doi:10.1016/j.enconman.2017.09.013.

[48] E. M. Zin and K. Bickford, "Feedforward Compensation in Multiple-Output DC/DC Converters," in *Proc. IEEE APEC*, 2012, pp. 1927–1933.

[49] Y. P. Siwakoti, F. Blaabjerg, and P. C. Loh, "Single-Inductor Multiple-Output DC–DC Converters—A Review," *IEEE Trans. Power Electron.*, vol. 34, no. 1, pp. 403–422, 2019, doi:10.1109/TPEL.2018.2821682.

[50] J. D. Dasika, B. Bahrani, M. Saeedifard, A. Karimi, and A. Rufer, "Multivariable Control of Single-Inductor Dual-Output Boost Converter," *IEEE Trans. Ind. Appl.*, vol. 50, no. 1, pp. 259–269, 2014, doi:10.1109/TIA.2013.2266616.